Improving the Execution Time of Large System Simulations

by

Nan Li

A Thesis Presented in Partial Fulfillment
of the Requirements for the Degree
Master of Science

Approved November 2012 by the
Graduate Supervisory Committee:

Daniel J. Tylavsky, Chair
Vijay Vittal
Kory W. Hedman

ARIZONA STATE UNIVERSITY

December 2012

ABSTRACT

Today, the electric power system faces new challenges from rapid developing technology and the growing concern about environmental problems. The future of the power system under these new challenges needs to be planned and studied. However, due to the high degree of computational complexity of the optimization problem, conducting a system planning study which takes into account the market structure and environmental constraints on a large-scale power system is computationally taxing.

To improve the execution time of large system simulations, such as the system planning study, two possible strategies are proposed in this thesis. The first one is to implement a relative new factorization method, known as the multifrontal method, to speed up the solution of the sparse linear matrix equations within the large system simulations. The performance of the multifrontal method implemented by UMFAPACK is compared with traditional LU factorization on a wide range of power-system matrices. The results show that the multifrontal method is superior to traditional LU factorization on relatively denser matrices found in other specialty areas, but has poor performance on the more sparse matrices that occur in power-system applications. This result suggests that multifrontal methods may not be an effective way to improve execution time for large system simulation and power system engineers should evaluate the performance of the multifrontal method before applying it to their applications.

The second strategy is to develop a small dc equivalent of the large-scale network with satisfactory accuracy for the large-scale system simulations. In this thesis, a modified Ward equivalent is generated for a large-scale power system, such as the full Electric Reliability Council of Texas (ERCOT) system. In this equivalent, all the generators in the full model are retained integrally. The accuracy of the modified Ward equivalent is validated and the equivalent is used to conduct the optimal generation investment planning study. By using the dc equivalent, the execution time for optimal generation investment planning is greatly reduced. Different scenarios are modeled to study the impact of fuel prices, environmental constraints and incentives for renewable energy on future investment and retirement in generation.

ACKNOWLEDGMENTS

I would like to express my sincere appreciation and gratitude to my advisor, Dr. Tylavsky, for his invaluable guidance and support throughout my graduate experience. He has always been a great source of encouragement and inspiration, helping and directing me to finish my research work and go through the tough times in my graduate study and life. I am always impressed by his responsibility towards this students and his dedication to profession and perfection.

I would also like to thank my committee members, Dr. Vijay Vittal and Dr. Kory Hedman for their valuable time and suggestions.

I am grateful to my parents for their endless love through all these years. Thanks for their faith and confidence in me, which gives me the courage to face up all the difficulties in my life.

In addition, I would like to thank the Power Systems Engineering Research Center and Consortium for Electric Reliability Technology Solutions for their financial support provided

Finally, I would like to thank all my friends I met here in Arizona State University. They would always be there standing by me when I needed them.

TABLE OF CONTENTS

Page

CHAPTER Page

CHAPTER Page

LIST OF TABLES

LIST OF FIGURES

Figure Page

Figure Page

NOMENCLATURE

a_{jk}	Emission cost vector at node *j* in hour *k*, $/tonne
α_i^{min}	Minimum generation for type *i*
ac	Alternating current
dc	Direct current
e_j	The j^{th} unit vector
BLAS	Basic Linear Algebra Subprograms
$c^F{}_i$	Cost of fuel, operations and maintenance per MWh for generator *i*
$c^I{}_i$	Annualized cost of new investment
$c^T{}_i$	Cost of taxes and insurance per MW for generator *i*
CHOLMOD	Supernodal sparse Cholesky factorization and update/downdate
Dis_{AB}	The electric distance between bus *A* and bus *B*
e_i	Emissions vector for generation type *i*, tonnes/MWh
EI	Eastern Interconnection
ERCOT	Electric Reliability Council of Texas
$Error_{Avg}$	Average error in the retained-line flows in MW
$Error_i$	Line-flow error in MW on retained line *i*
$Error_i\%$	Line-flow error in percentage on retained line *i*
GHG	Greenhouse gas
GPLU	A LU factorization algorithm developed by Gilbert and Peierls
H_k	Number of hours that system is at load profile *k*

HVDC	High-voltage direct current
I_{Gi}	Generator output current at bus *i*
I_{ij}	Capacity investment for generator *i* at node *j*
I_{Li}	Load current at bus *i*
K_{ij}	Max investment in fuel type *i* at node *j*
LAPACK	Linear Algebra Package
L_{jk}	Net load
LMP	Locational marginal price
LTC	Load tap change
MMWG	Multi-regional Modeling Working Group
$(Lim_{MVA})_i$	MVA rating of transmission line *i*
n	Number of buses in the reduced network
N_r	Number of retained lines in the reduced model
NB_i	Number of buses that are directly connected to bus *i* in the equivalent network
OPF	Optimal power flow
p^0_{ij}	Existing generator capacity
p_{ijk}	Aggregate real power output from generator *i* at node *j* during representative hour *k*
P_{ac_from}	Power flow at the sending end of a HVDC line (at the ac side of the converter)
P'_{ac_from}	Power injection at the equivalent generator at the sending end of a HVDC line
P_{ac_to}	Power flow at the receiving end of a HVDC line (at the ac side of the converter)

`

P'_{ac_to}	Power injection at the equivalent generator at the receiving end of a HVDC line
P_{dc_from}	Power flow at the sending end of a HVDC line (at the dc side of the converter)
P_{Loss}	Power loss on a HVDC line
P_{dc_to}	Power flow at the receiving end of a HVDC line (at the dc side of the converter)
PF	Power flow
P_{flow}	*L*-by-1 branch power flow vector
Pf_i^{full}	Power flow on transmission line *i* in the full model
$Pf_i^{reduced}$	Power flow on transmission line *i* in the reduced model
PFLOW	Power flow program developed at University of Waterloo
p_{Gi}	Active power output of generator *i* in MW
P_{Gi}	Active power output of a generator at bus *i*
P_{Li}	Active power component of a load at bus *i*
PTDF	Power transfer distribution factor
Q_{Gi}	Reactive power output of a generator at bus *i*
Q_{Li}	Reactive power component of a load at bus *i*
R_{ij}	Capacity requirement for generator *i* at node *j*
RGGI	Regional Greenhouse Gas Initiative
$r_{k_i\_j}$	The resistance of the j^{th} transmission line in path k_i
REI	Radial equivalent independent
SVC	Static VAR compensator

`

TL	Transmission line
V_i	Voltage at bus i
UMFPACK	Unsymmetric multifrontal sparse LU factorization package
WECC	Western Electricity Coordinating Council
$x_{k_i\_j}$	The reactance of the j^{th} transmission line in path k_i
θ	N-by-1 vector containing the bus voltage angles of the full system
λ_i	The multiplier for loss compensation in zone i
$\alpha_i^{min\ n}$	Minimum generation for type i
$(\cdot)^T$	Transpose of a matrix

CHAPTER 1 .

INTRODUCTION

1.1 Background Introduction

With rapid development of new technology and the growing concern regarding climate change, the power system today faces new challenges. One of them is the environmental challenge brought on by the global warming. Climate change resulting from greenhouse gases (GHGs) poses a huge threat to human welfare [1], [2], and CO_2 contributes to 77% of the greenhouse gas effect. To prevent global warming from further worsening, many actions have been taken in recent years. The Kyoto protocol was entered into force on February 16, 2005. As of May 2008, 182 parties have ratified the protocol to combat global warming [3]. In United States, 39 states in U.S. had developed action plans aiming at greenhouse gas emission reductions. In northeastern America, 9 states have participated in the regional greenhouse gas initiative (RGGI) which is aimed at reducing greenhouse emissions from the power plants. RGGI utilizes a CO_2 Budget Trading Program to regulate CO_2 emissions from fossil fuel plants and the goal is to reduce CO_2 emissions in the nine participating states by 10 percent by 2018. Another environmental challenge is due to the tightened standards on NO_2 and SO_2 emission, which are regulated by the cross-state air-pollution rule.

Besides the environmental challenges, the electric-power industry also faces challenges from the rapid development of technology. Such challenges include the possibility of increased demand from plug-in hybrids, increased demand from energy consumers trying to seek cheaper and cleaner energy, and the increasing

penetration of renewable energy. The new challenges, taken together, have the potential to radically change the way the power system is operated and designed. Therefore, the future of the power system under these new challenges needs to be planned and studied.

Conducting system planning studies for a large-scale power system which takes into account of the market structure and environmental regulations is prohibitively expensive in terms of computational time. Due to the number of endogenous variables, number of equality and inequality constraints, and network model size, the optimization problem has a high degree of computational complexity. For example, on a state-of-art PC, it may take more than 48 hours of execution time to solve an optimal generation-investment planning problem (for a 6000-bus system) which includes consideration of multiple scenarios and modeling of generation contingency and environmental constraints. To solve the same problem for larger systems, the execution time will increase more than linearly as the size of system grows.

Therefore, to reduce the execution time of simulation with large system, a practical way is to use a small, dc equivalent of the large-scale network with satisfactory accuracy. In this thesis, a backbone equivalent for a large-scale power system, such as the ERCOT system, is developed using a novel network reduction scheme.

Besides developing an equivalent for a large-scale system, another possible strategy to reduce the execution time of large system simulation is to improve the computational efficiency of the sparse linear solvers. In the interest of speeding up

packages like the SuperOPF, this thesis also presents a study on a relatively new factorization method, known as the multifrontal method, which is touted as having the potential to significantly speed up the solution of the sparse linear matrix equation problem. Explained in the thesis are the fundamental concepts central to multifrontal methods and the multifrontal method is tested on different types of matrices. The performance of the multifrontal method on different types of matrices is compared to the traditional LU factorization and the results are presented.

1.2 Summary of Chapters

In chapter 2, the development of multifrontal methods and its application in power system is reviewed. The formulations of the multifrontal method and the central concept upon which they are based are introduced. The efficiency of the multifrontal method is compared against traditional LU factorization on different types of matrices and a discussion of the results is presented.

In chapter 3, the method used for developing the dc backbone equivalent for a large-scale power system is described. A brief introduction to the ERCOT system is given and a backbone equivalent for the ERCOT system is generated.

In chapter 4, the accuracy of the ERCOT equivalent model is evaluated in terms of dc power flow (PF) and dc optimal power flow (OPF). A study of the accuracy of the dc power flow model is presented.

In chapter 5, the backbone equivalent for the ERCOT system is implemented in SuperOPF to conduct optimal generation planning study which takes into

account of environmental regulations. The effect of different polices are studied and a discussion of the results is presented.

In chapter 6, conclusions to this thesis and a discussion of the future work are presented.

CHAPTER 2 .

MULTIFRONTAL METHODS

This chapter presents a study of a factorization method that is touted as having the potential to speed up triangular factorization packages that are used in large-scale system simulation and analysis packages. The background and motivation of the study is introduced in the beginning of this chapter. Then the development of the multifrontal method and its previous application to power system problems is reviewed. The fundamental concepts needed to understand multifrontal methods are introduced and examples are provided to illustrate these concepts. Finally, the chapter compares the performance of the multifrontal method and traditional LU factorization on different types of matrices and presents a discussion of the results.

2.1 Background and Motivation of the Study on the Multifrontal Method

The solution of $Ax=b$ is pervasive in power system simulations. In planning tools like the SuperOPF, the solution of sparse linear algebraic equations is inevitable, since the package will solve the power flow (PF) and OPF problems. In large, the execution time of solving sparse linear algebra equations comprises a considerable portion of the total simulation time. Therefore, speeding up the solution of sparse linear algebraic equations has the potential to greatly reduce the total execution time required by packages used in system planning studies.

Much research into the solution of sparse linear matrix equations, $Ax=b$, by power-system researchers has led to the consensus that the so-called traditional sparse matrix methods for LU factorization are the fastest direct methods when

applied to matrices characteristic of power-system simulations. Recently, claims [22] have been made that the multifrontal method provides a speedup factor of over five in solving power-system time-domain simulation problems. The speedup of this order of magnitude would represent a quantum leap in sparse matrix and vector technology. Therefore, the objective of this study is to independently verify the efficiency of the multifrontal method in power system problems and its applicability in improving computational efficiency of solving sparse linear algebraic equation $Ax=b$.

2.2 Literature Review of Multifrontal Methods

The multifrontal method developed by Duff and Reid in 1983, is a direct method for the sparse matrix solution [6] that carries out the factorization of a sparse matrix by factoring small dense frontal matrices in a specific sequence.

The term "multifrontal" is first used by Duff and Reid [7], since multifrontal method is a generalization of the frontal method of Irons [8]. For many years, the multifrontal method has been widely used in different applications [7], [9], [10]. Its effective usage has been reported many times in the literature, such as in the solution of separable optimization problems [11], in semi-conductor device simulations [12], in the solution for computational fluid dynamics [13], as well as in power-system power flow and time domain dynamic simulations [20]-[22].

Many papers have reported research on the development and improvement of multifrontal methods. A review of them follows.

Reference [15] reported development on a combined unsymmetric unifrontal/multifrontal method. This combined method improved some of the

drawbacks of the unifrontal and multifrontal methods: it reduced the overhead of data movement with multifrontal methods, and overcame the weakness with unifrontal methods—unifrontal methods usually yield a large number of fill-ins for matrices with large profiles [15], [16]. This combined method was tested on unsymmetric matrices with a degree of structural symmetry of less than 0.3[1] and matrices with more than 6 nonzeros per row, and its performance was compared with the traditional multifrontal methods [29], [30], traditional unifrontal method [31] and traditional LU factorization. The results showed that the combined method improved computational efficiency and reduced memory requirements as the degree of unsymmetric and density increased.

Reference [17] presented a factorization method that combines a column pre-ordering strategy with a right-looking unsymmetric multifrontal factorization method. This method first analyzes the matrix to determine whether the nonzero pattern of the matrix is symmetric or unsymmetric. Once the nonzero pattern of the matrix is determined, the method chooses one of the three following strategies to pre-order the rows and columns: unsymmetric, 2-by-2, and symmetric. Then based on a supernodal elimination tree, the factorization of the matrix is broken down into the factorization of a sequence of dense frontal matrices. The proposed method was compared against other algorithms and the results showed that the proposed method is superior to other methods on a wide range of matrices [17].

[1] The degree of structural symmetry is the ratio of the number of matched off-diagonal entries to the total number of off-diagonal entries. An entry a_{ij} ($i \neq j$) is called matched if both a_{ij} and a_{ji} is nonzero.

However, [17] did not show if the performance of multifrontal method was related to the degree of sparsity of the matrices.

The application of multifrontal methods to power system problems was presented in [20]-[22]. In reference [20], the focus of the study was to develop an automatic code-differentiation tool for power-flow solutions. A multifrontal-method-based package, UMFPACK [23], was used in the study of the solution of sparse linear equations, and the study showed its performance was superior to a linear solver from the power-flow program PFLOW [24]. However, [20] did not provide any information on what optimal ordering scheme was used, or the number of fill-ins yielded in UMFPACK and the solver from PFLOW.

The multifrontal method was also applied in reference [21] as a sparse linear solver for power flow problems. However, the focus of [21] was to promote FPGA technology as a hardware implementation for sparse linear solver, rather than the software solution using a multifrontal method. Reference [21] compared the performance of UMFPACK with two other packages and claimed that UMFPACK gave the best results. However, no details about these packages were presented in the paper, such as the type of optimal ordering scheme used or the number of fill-ins yielded by each package, or the structure of the code or a comparison of the data structures used.

Reference [22] presented the application of UMFPACK [23] in power system dynamic simulations. In [22], UMFPACK was used to solve discretized-differential and linear algebraic equations that occur in power-system dynamic simulations. The study showed that multifrontal method achieved much higher

computational efficiency as compared to other sparse linear solvers, such as GPLU [27], CHOLMOD [25] and a sparse LU factorization routine whose kernel was from LAPACK [26]. However, reference [22] did not show if these solvers were using the same optimal ordering scheme, or the numbers of fill-ins generated by each solver are same or close.

2.3 Fundamental Principles of Multifrontal Methods

For those somewhat familiar with multifrontal methods, this section provides a quick review of the approach. For those new to multifrontal methods, this section provides an overview of the algorithm, introducing some of the terms that will be defined in the subsequent subsections.

The multifrontal method is a direct method for the solution of sparse matrix equations that processes operations needed in the triangular factorization in a sequence of small dense frontal matrices based on the precedence relationships imposed by an elimination tree and an optimal ordering, such as the minimum degree [70]. Each node of the elimination tree represents a small dense frontal matrix. Each frontal matrix holds one or more pivot rows and columns. The frontal matrices are processed from leaf to root obeying the precedence relationships implied by the elimination tree. At each node of the elimination tree, the factorization kernel is processed in the following sequence. First, the original entries corresponding to rows and columns in matrix A are assembled into the current frontal matrix. If there are any prior contribution blocks from the descendants of the current node, the contribution blocks are assembled into the current frontal matrix by an assembly step. After the assembly step, one or more

steps of LU factorization are performed within the current frontal matrix and a contribution block (a Schur complement) is computed. This contribution block is placed on a stack and is used in subsequent steps in eliminating the parent of the current node in the elimination tree.

In the following subsections, the key definitions used in describing the many variants of the multifrontal method are introduced. They are the elimination tree, the frontal matrix, the update matrix, the extend-add operation and the supernode partition.

2.3.1. Elimination Tree Structure

The elimination tree plays an important role in sparse matrix factorization and is familiar to power-system engineers experienced with the application of sparsity methods to the linear matrix problem. It determines the processing sequence of the sparse matrix factorization. In the symbolic factorization phase, once the factor matrix structure is obtained, the elimination tree can be formed. The notation $T[j]$ is used to represent a set of nodes that contains node j and its descendants in the elimination tree. In other words, $T[j]$ contains node j and the set of nodes in the subtree rooted at node j.

To illustrate this, consider a symmetric positive definite irreducible matrix A and its factor matrix L as shown in Fig. 2.1. Each "•" in Fig. 2.1represents an original nonzero entry in matrix A, and each "×" represents a fill-in in the factor matrix L. The elimination tree corresponding to the matrix A is shown in Fig. 2.2. The notation T[2] when applied to Fig. 2.1, represents the set of T[2]={1,2}, and

T[6] corresponds to the set of T[6]={3,4,5,6}. The detailed definition of the elimination tree and other examples can be found in [34].

$$A = \begin{array}{c} 1 \\ 2 \\ 3 \\ 4 \\ 5 \\ 6 \\ 7 \\ 8 \\ 9 \end{array} \begin{pmatrix} a & \bullet & & & & & \bullet & \bullet & \\ \bullet & b & & & & & \bullet & \bullet & \\ & & c & \bullet & & & & & \bullet \\ & & \bullet & d & & \bullet & & & \\ & & & & e & \bullet & \bullet & & \bullet \\ & & & \bullet & \bullet & f & & \bullet & \\ \bullet & \bullet & & & \bullet & & g & & \bullet \\ \bullet & \bullet & & & & \bullet & & h & \\ & & \bullet & & \bullet & & \bullet & & i \end{pmatrix}$$

$$L = \begin{array}{c} 1 \\ 2 \\ 3 \\ 4 \\ 5 \\ 6 \\ 7 \\ 8 \\ 9 \end{array} \begin{pmatrix} a & & & & & & & & \\ \bullet & b & & & & & & & \\ & & c & & & & & & \\ & & \bullet & d & & & & & \\ & & & & e & & & & \\ & & & \bullet & \bullet & f & & & \\ \bullet & \bullet & & & \bullet & \times & g & & \\ \bullet & \bullet & & & & \bullet & \times & h & \\ & & \bullet & \times & \bullet & \times & \bullet & \times & i \end{pmatrix}$$

Fig. 2.1 An example sparse matrix and its lower triangular factor

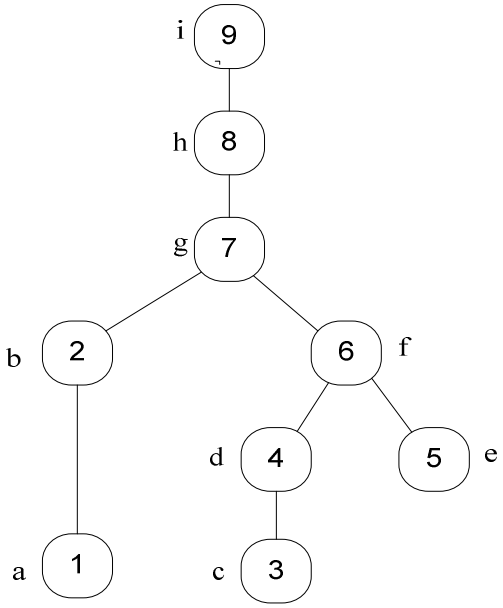

Fig. 2.2 Elimination tree for matrix *A*

2.3.2. Frontal Matrices and Update Matrices

The subtree update matrix of node *j* is defined to be the matrix that contains the outer-product of nonzero contributions from the descendants of node *j*. For sparse matrix *A* and its factor matrix *L*, the subtree update matrix at node *j* can be represented as

$$\bar{U}_j = -\sum_{k \in T[j]-\{j\}} \begin{pmatrix} l_{j,k} \\ l_{i_1,k} \\ \vdots \\ l_{i_r,k} \end{pmatrix} \begin{pmatrix} l_{k,j} & l_{k,i_1} & \cdots & l_{k,i_r} \end{pmatrix} \tag{2.1}$$

where

$$\{i_1, i_2, \cdots, i_r\} = \{i > j \mid l_{ik} \neq 0\} \tag{2.2}$$

and where it is assumed that there are *r* below-diagonal nonzero elements in column *j* of *L*.

The frontal matrix of node *j* is defined to be the matrix

$$F_j = \begin{pmatrix} a_{j,j} & a_{j,i_1} & \cdots & a_{j,i_r} \\ a_{i_1,j} & & & \\ \vdots & & 0 & \\ a_{i_r,j} & & & \end{pmatrix} + \bar{U}_j \tag{2.3}$$

Constructing this frontal matrix represents a cost penalty (more execution time and more storage) for the multifrontal method when compared with the traditional LU factorization since no counterpart matrix is needed with the traditional LU factorization. The F_j matrix is a composite of the original elements in column and row *j* of matrix *A* and the elements from the update matrices of the descendants of node *j*. Both $\bar{U}_j$ and F_j are of dimension (*r* + 1), which equals the number of nonzeros in column *j* of the factor matrix *L*. Once F_j is formed, all the necessary modifications have been made to the first column/row of F_j and all the nonzero contributions from the descendants of node *j* have been assembled into F_j.Therefore F_j is ready to be factored.

F_j can be factored into the following form:

$$F_j = \begin{pmatrix} l_{j,j} & 0 \\ l_{i_1,j} & \\ \vdots & I \\ l_{i_r,j} & \end{pmatrix} \begin{pmatrix} 1 & 0 \\ 0 & U_j \end{pmatrix} \begin{pmatrix} l_{j,j} & l_{j,i_1} & \cdots & l_{j,i_r} \\ 0 & & I & \end{pmatrix} \tag{2.4}$$

The vector $(l_{j,j}, l_{i_1,j}, ..., l_{i_r,j})^t$ contains the nonzero entries in column *j* of factor matrix *L*. The matrix U_j, referred to as the update matrix from node *j*, is

$$U_j = -\sum_{k \in T[j]} \begin{pmatrix} l_{i_1,k} \\ \vdots \\ l_{i_r,k} \end{pmatrix} \begin{pmatrix} l_{k,i_1} & \cdots & l_{k,i_r} \end{pmatrix} \tag{2.5}$$

After F_j is factored as in (2.4), U_j keeps the structure and update information from node j and its descendants. In other words, U_j is ready to be used to assemble the frontal matrix for the parent of node j.

2.3.3. Extend-add Operation and Formation of Frontal Matrix

By definition of (2.3), the frontal matrix consists of two parts. The first term F_j is formed directly from matrix A. The second part $\bar{U}_j$ is the subtree update matrix at node j, which is obtained by accumulating the outer-product matrices from the descendants of node j. The process of accumulation of $\bar{U}_j$ can be represented by using the so-called "extend-add" operation [6]. The extend-add operation can be explained using the following example.

Let H be an h by h matrix with $h \le n$, and G be a g by g matrix with $g \le n$. Each row/column of H and G corresponds to a row/column of a given n by n matrix M. Let $i_1 \le i_2 \le \cdots \le i_h$ be the subscripts of H in M, and $j_1 \le j_2 \le \cdots \le j_g$ be those of G in M. Let $k_1, k_2, k_3, ..., k_t$ be the union of the two subscript sets. The matrix H and G can be extended to conform to the subscript set $\{k_1, k_2, k_3, ..., k_t\}$ by introducing a number of zero rows and columns in H and G. Here, we define $H \dotplus G$ to be the t-by-t ($t \le h+g$) matrix formed by adding the two extended matrices of H and G. And the operator "$\dotplus$" is referred to as matrix extend-add operator.

For example, let

$$H = \begin{pmatrix} m & n \\ p & q \end{pmatrix}, G = \begin{pmatrix} w & x \\ y & z \end{pmatrix} \tag{2.6}$$

and let {1,2} and {1,3} be the subscript sets of matrix H and G, respectively. Then by definition, $H \dotplus G$ is

$$H \dotplus G = \begin{pmatrix} m & n & 0 \\ p & q & 0 \\ 0 & 0 & 0 \end{pmatrix} \dotplus \begin{pmatrix} w & 0 & x \\ 0 & 0 & 0 \\ y & 0 & z \end{pmatrix}$$

$$= \begin{pmatrix} m+w & n & x \\ p & q & 0 \\ y & 0 & z \end{pmatrix} \tag{2.7}$$

By using the extend-add formulation, F_j in (2.3) can be rewritten in terms of update matrices as

$$F_j = \begin{pmatrix} a_{j,j} & a_{j,i_1} & \cdots & a_{j,i_r} \\ a_{i_1,j} & & & \\ \vdots & & 0 & \\ a_{i_r,j} & & & \end{pmatrix} \dotplus U_{c_1} \dotplus \ldots \dotplus U_{c_s} \tag{2.8}$$

where subscripts $c_1,\ldots,c_s$ correspond to the descendants immediately rooted at node j in the elimination tree, and U_{c_j} $\mathrm{U_{cj}}$ represent the corresponding update matrices contributed by these descendants. Here we define the nodes that are immediately rooted under node j in the elimination tree to be the children of node j. For example, for node 6, node 3, 4 and 5 are all its descendants but only node 4 and 5 are its children. Note that the update matrix from a child of node j includes the relevant elimination information from all descendants in the subtree rooted at

this child node. Also note that matrices $U_{c_1},\ldots,U_{c_s}$ may not be conformable, and the purpose of the extend-add operation is to expand all matrices to make them conformable and perform the matrix accumulation. This expansion to get conformable matrices represents work not needed with the traditional LU factorization.

2.3.4. Example Multifrontal Method Process

To illustrate the procedure of the multifrontal method, consider the factorization step of node 6. Before eliminating node 6, node 3, 4 and 5 should be eliminated and U_4 and U_5 are needed to build the frontal matrix F_6. It is easy to see that T[3]={3} and T[5]={5}, so the elimination steps on node 3 and node 5 do not need contribution blocks from other nodes. Since T[4]={3,4}, $\bar{U}_4$ is given by the update matrix U_3, which is

$$U_3 = -\begin{pmatrix} l_{43}l_{34} & l_{43}l_{39} \\ l_{93}l_{34} & l_{93}l_{39} \end{pmatrix} = -\begin{pmatrix} l_{43} \\ l_{93} \end{pmatrix}\begin{pmatrix} l_{34} & l_{39} \end{pmatrix} \tag{2.9}$$

Based on (2.3), F_4 is formed as

i EMBED Equation.DSMT4

$$F_4 = \begin{pmatrix} a_{44} & a_{46} & 0 \\ a_{64} & 0 & 0 \\ 0 & 0 & 0 \end{pmatrix} + \bar{U}_4$$

$$= \begin{pmatrix} a_{44} & a_{46} & 0 \\ a_{64} & 0 & 0 \\ 0 & 0 & 0 \end{pmatrix} \dot{+} U_3 \tag{2.10}$$

$$= \begin{pmatrix} a_{44} - l_{43}l_{34} & a_{46} & -l_{43}l_{39} \\ a_{64} & 0 & 0 \\ -l_{93}l_{34} & 0 & -l_{93}l_{39} \end{pmatrix}$$

After the first row and column of F_4 are eliminated, the update matrix U_4 is given by,

$$\begin{aligned} U_4 &= \begin{pmatrix} -l_{64}l_{46} & -l_{64}l_{49} \\ -l_{94}l_{46} & -l_{93}l_{39} - l_{94}l_{49} \end{pmatrix} \\ &= -\begin{pmatrix} l_{64} \\ l_{94} \end{pmatrix} \begin{pmatrix} l_{46} & l_{49} \end{pmatrix} - \begin{pmatrix} 0 \\ l_{93} \end{pmatrix} \begin{pmatrix} 0 & l_{39} \end{pmatrix} \end{aligned} \tag{2.11}$$

Since $T[5]=\{5\}$, F_5 is formulated as

$$F_5 = \begin{pmatrix} a_{55} & a_{56} & a_{57} & a_{59} \\ a_{65} & 0 & 0 & 0 \\ a_{75} & 0 & 0 & 0 \\ a_{95} & 0 & 0 & 0 \end{pmatrix} \tag{2.12}$$

and the update matrix U_5 is given by

$$\begin{aligned} U_5 &= \begin{pmatrix} -l_{65}l_{56} & -l_{65}l_{57} & -l_{65}l_{59} \\ -l_{75}l_{56} & -l_{75}l_{57} & -l_{75}l_{59} \\ -l_{95}l_{56} & -l_{95}l_{57} & -l_{95}l_{59} \end{pmatrix} \\ &= -\begin{pmatrix} l_{65} \\ l_{75} \\ l_{95} \end{pmatrix} \begin{pmatrix} l_{56} & l_{57} & l_{59} \end{pmatrix} \end{aligned} \tag{2.13}$$

By using the extend-add operation defined by (2.8), F_6 can be written in the form:

$$F_6 = \begin{pmatrix} a_{66} & 0 & a_{68} & 0 \\ 0 & 0 & 0 & 0 \\ a_{86} & 0 & 0 & 0 \\ 0 & 0 & 0 & 0 \end{pmatrix} \dotplus U_4 \dotplus U_5$$

$$= \begin{pmatrix} a_{66} & 0 & a_{68} & 0 \\ 0 & 0 & 0 & 0 \\ a_{86} & 0 & 0 & 0 \\ 0 & 0 & 0 & 0 \end{pmatrix} \dotplus \begin{pmatrix} -l_{64}l_{46} & -l_{64}l_{49} \\ -l_{94}l_{46} & -l_{93}l_{39} - l_{94}l_{49} \end{pmatrix}$$

$$\dotplus \begin{pmatrix} -l_{65}l_{56} & -l_{65}l_{57} & -l_{65}l_{59} \\ -l_{75}l_{56} & -l_{75}l_{57} & -l_{75}l_{59} \\ -l_{95}l_{56} & -l_{95}l_{57} & -l_{95}l_{59} \end{pmatrix}$$

$$= \begin{pmatrix} a_{66} - l_{64}l_{46} - l_{65}l_{56} & -l_{65}l_{57} & a_{68} & -l_{64}l_{49} - l_{65}l_{59} \\ -l_{75}l_{56} & -l_{75}l_{57} & 0 & -l_{75}l_{59} \\ a_{86} & 0 & 0 & 0 \\ -l_{94}l_{46} - l_{95}l_{56} & -l_{95}l_{57} & 0 & -l_{93}l_{39} - l_{94}l_{49} - l_{95}l_{59} \end{pmatrix} \qquad (2.14)$$

After the first row and column in F_6 are eliminated, the update matrix U_6 is given by

$$U_6 = \begin{pmatrix} -l_{75}l_{57} - l_{76}l_{67} & -l_{76}l_{68} & -l_{75}l_{59} - l_{76}l_{69} \\ -l_{86}l_{67} & -l_{86}l_{68} & -l_{86}l_{69} \\ -l_{95}l_{57} - l_{96}l_{67} & -l_{96}l_{68} & -l_{93}l_{39} - l_{94}l_{49} - l_{95}l_{59} - l_{96}l_{69} \end{pmatrix} \qquad (2.15)$$

Or U_6 can be represented in terms of outer-product updates contributed by nodes in set T[6]={3,4,5,6},which is

$$U_6 = -\begin{pmatrix} 0 \\ 0 \\ l_{93} \end{pmatrix}\begin{pmatrix} 0 & 0 & l_{39} \end{pmatrix} - \begin{pmatrix} 0 \\ 0 \\ l_{94} \end{pmatrix}\begin{pmatrix} 0 & 0 & l_{49} \end{pmatrix}$$
$$- \begin{pmatrix} l_{75} \\ 0 \\ l_{95} \end{pmatrix}\begin{pmatrix} l_{57} & 0 & l_{59} \end{pmatrix} - \begin{pmatrix} l_{76} \\ l_{86} \\ l_{96} \end{pmatrix}\begin{pmatrix} l_{67} & l_{68} & l_{69} \end{pmatrix} \qquad (2.16)$$

2.3.5. The Supernode Partition

The supernode partitioning, [7], [19], plays a significant role in most variants of the multifrontal method. Supernode partitioning has also been referred to as “supervariable” [14] and “indistinguishable node” [38]in the literature.

Generally speaking, a supernode is a group of columns/rows that share an identical sparsity structure. Assume node k is a descendant of node j in the elimination tree and let $C[k]$ represent the set of column indices of the nonzeros in column k in factor matrix L, and let $C[j]$ represent the set of column indices of the nonzeros in column j in factor matrix L. If $C[j]=C[k]-\{k\}$, then in this case, node k and j can form a supernode. If k is eliminated, its update matrix U_k has nonzero row and column indices corresponding exactly to the nonzero row and column indices of the frontal matrix F_j. Therefore nodes k and j can be eliminated together as a supernode $\{k, j\}$ and the step of assembling U_k into F_j has been avoided.

For the matrix in Fig. 2.1 with the given ordering, five supernodes can be obtained, given by:

$$\{1,2\},\{3\},\{4\},\{5\},\{6,7,8,9\}$$

Partitioning the nodes into supernodes provides significant computational advantages when integrated into multifrontal methods. By using supernode

partitions, all nodes in a supernode share the same frontal matrix F_j and are updated together by update matrices U_c from the children of supernode j. Once the frontal matrix is formed, the nodes in the supernode j can be eliminated together as a unit. The total number of frontal matrices assembled during factorization is thereby reduced from the number of the nodes to the number of the supernodes.

The supernode partitioning scheme introduced above requires all nodes in a supernode to have the identical sparsity structure. However sometimes the computational gain obtained by this version of supernode partitioning is small. Reference [19]proposed a relaxed supernode partitioning scheme. The relaxed supernode partition allows zero entries to be introduced into the supernode. For example, by using relaxed supernode partition, node 3 and 4 can be grouped as a supernode, in which case the zero entry a_{63} will be introduced into supernode $\{3,4\}$. Similarly, node 5, 6, 7, 8 and 9 can also form a supernode by introducing zero entry a_{85} into the supernode.

The supernode algorithm enables the multifrontal method to take advantage of the repetitive structure in the matrix by processing more than one column/row in each frontal matrix. Thus the “supernode multifrontal method” can fully take advantage of the high performance computer architecture by using Level 3 BLAS [18] in its innermost loops.

2.4 Numerical Results

2.4.1. Experiment Design

In this section, the design of the experiment used to compare the performance of multifrontal factorization with the traditional LU factorization is described and the results are presented.

The goal of our experiment was to compare the performance of the multifrontal factorization approach from UMFPACK [23] with a traditional LU factorization program of our own design coded using C++. UMFPACK is a set of ANSI/ISO C routines for solving unsymmetric sparse linear systems, $Ax=b$, using the unsymmetric multifrontal method. It is one of the prominent software packages for solving general sparse matrix problems.

The experiment was carried out on a Dell OPTIPLEX 780 with a 3.16 GHz Core 2 processor, 3 GB of RAM and 6MB cache. ATLAS [39] was used with UMFPACK.

The node ordering in the matrices we used for test purposes was determined by using the AMD (approximate minimum-degree) [33] algorithm to minimize fill-ins. The AMD ordering was applied to the test matrices before being processed by either UMFPACK or the traditional LU routine we developed, so that the two solvers yielded exactly the same number of fill-ins for each matrix.

TABLE 2.1
EXECUTION TIME FOR NUMERICAL FACTORIZATION OF POWER SYSTEM BUS ADMITTANCE MATRICES

Size	Nonzeros in A	Nonzeros per Row in A	Nonzeros in L and U Factors	Numerical Factorization Execution Time (sec.)		UMFPACK Gain
				UMFPACK	LU	
662	2474	3.74	4436	0.00239	0.00031	0.13
1138	4054	3.56	5392	0.00362	0.00037	0.10
4578	28546	6.24	60942	0.01942	0.00959	0.49
6054	20346	3.36	35698	0.01857	0.00291	0.16
59046	200761	3.40	399848	0.18512	0.0346	0.19

TABLE 2.2
EXECUTION TIME FOR NUMERICAL FACTORIZATION OF STRUCTURAL MATRICES

Size	Nonzeros in A	Nonzeros per Row in A	Nonzeros in L and U Factors	Numerical Factorization Execution Time (sec.)		UMFPACK Gain
				UMFPACK	LU	
1074	12957	12.06	61209	0.01159	0.02878	2.48
3562	159910	44.89	573744	0.07012	0.45003	6.42
5489	217651	39.65	1064975	0.14645	1.08846	7.43
7102	340200	47.90	738823	0.10299	0.46234	4.49
10848	1229776	113.36	3922038	0.67739	7.15113	10.56

TABLE 2.3
EXECUTION TIME FOR NUMERICAL FACTORIZATION OF POWER FLOW JACOBIAN MATRICES

Size	Nonzeros in A	Nonzeros per Row in A	Nonzeros in L and U Factors	Numerical Factorization Execution Time (sec.)		UMFPACK Gain
				UMFPACK	LU	
1324	9896	7.47	17592	0.0051	0.0016	0.32
2276	16216	7.12	21495	0.0075	0.0015	0.20
9156	114184	12.47	244695	0.0479	0.0650	1.36
12108	81384	6.72	141408	0.0444	0.0163	0.37
118092	800704	6.78	1419721	0.4910	0.2300	0.47

TABLE 2.4
EXECUTION TIME FOR NUMERICAL FACTORIZATION OF NORMAL-FORM STATE ESTIMATION MATRICES

Size	Nonzeros in A	Nonzeros per Row in A	Nonzeros in L and U Factors	Numerical Factorization Execution Time (sec.)		UMFPACK Gain
				UMFPACK	LU	
662	6480	9.79	15376	0.00390	0.00251	0.64
1138	11142	9.79	16628	0.00592	0.00210	0.35
4578	100590	21.97	258604	0.06459	0.11095	1.72
6054	50706	8.38	129020	0.06082	0.02549	0.42
59046	511858	8.67	1349936	1.24664	0.42633	0.34

TABLE 2.5
EXECUTION TIME FOR NUMERICAL FACTORIZATION OF DYNAMIC SIMULATION JACOBIAN MATRICES

Size	Nonzeros in A	Nonzeros per Row in A	Nonzeros in L and U Factors	Numerical Factorization Execution Time (sec.)		UMFPACK Gain
				UMFPACK	LU	
749	2926	3.91	3409	0.00206	0.00031	0.15
7984	43888	5.50	53797	0.02070	0.00382	0.18
76859	360644	4.69	471113	0.25084	0.04028	0.16

Table 2.1 through Table 2.5 show the characteristics of the five sets of test matrices we acquired. Each table lists the structural information for each set of matrices, namely the matrix dimension, number of nonzeros in matrix *A*, number of nonzeros per row in *A* and the sum of nonzeros in *L* and *U* factors for each matrix. The matrices in Table 2.1 are incident-symmetric bus admittance matrices for typical power system topologies (with typically 3-4 nonzeros per row). Note that the 4578 node matrix has 6 nonzeros per row. This matrix is a reduced equivalent generated using the 59,046 bus system and has many equivalent lines. The second set of matrices is obtained from the University of Florida Sparse Matrix Collection [40], as shown in Table 2.2. The matrices contained in Table 2.2 are structural problem matrices which are incident-symmetric and much denser than power system matrices. The third set of matrices, as shown in Table 2.3, contains incident-symmetric power-flow Jacobian matrices. Matrices in this set are created from the matrices in the first set and typically have two times the number of nonzeros per row as the matrices in the first set. The matrices in the fourth set are matrices in the form of A^TA, which occur in the normal-form formulation of power system state estimation problem. While it is rare to solve the normal-form formulation of the state estimation problem because of the attendant ill-conditioning, we applied the multifrontal method and traditional LU

factorization to evaluate the comparative performance of the algorithms on these denser matrices which have sparsity patterns characteristic of power system problems. Table 2.5 shows the last set of matrices, which are matrices characteristic of short-term dynamic simulations. With exception of the last set of matrices, all the matrices in the first four sets are incident but not necessarily numerically symmetric. Matrices in the last set are both incident and numerically asymmetric. We have blocked pivoting for all the power-system matrices, since pivoting is rarely necessary when factoring matrices characteristic of power system problems. Pivoting is also blocked for structural problem matrices, since all the matrices in Table 2.2 are positive definite. UMFPACK is a package designed for unsymmetric matrices; therefore, to conduct a fair comparison, in the traditional LU factorization code we designed, all the matrices were treated as numerically asymmetric.

2.4.2. Experiment Results and Results Analysis

For the matrices of Table 2.1, the numerical factorization execution times for UMFPACK and our LU routine are shown for each matrix in Table 2.1. The ratio of numerical factorization time of traditional LU method to that of UMFPACK is also shown in Table 2.1. This ratio shows that traditional LU factorization is superior to UMFPACK's multifrontal method for matrices with the sparsity degree and structure of power-system admittance matrices. It is interesting to note that for the 4578 bus matrix, which has approximately 6 nonzeros per row, the UMFPACK gain decreases, suggesting that, as matrices become denser, the multifrontal method may become competitive.

Results in Table 2.2 show that for relatively denser matrices whose sparsity structure is different from those of power system matrices and whose rows have on the average of more than 10 nonzeros, the multifrontal method becomes superior to the traditional LU factorization. The speed up of the multifrontal method over the traditional LU factorization method varies between 2.4 to 10.6 times for these denser matrices. The result from Table 2.2 again suggests that the multifrontal method will become competitive as matrices become denser.

The results for the third and fourth set of matrices are shown in Table 2.3 and Table 2.4. For the matrices with 6 to 10 nonzeros per row as shown in Table 2.3 and Table 2.4, traditional LU factorization is found to be more efficient than the multifrontal method. Comparison of the UMFPACK gains in Table 2.3 and Table 2.4 to the UMFPACK gains in Table 2.1, again suggests that the UMFPACK gains increase as matrices become denser. It should be noted that the 9156 node matrix in Table 2.3 and the 4578 node matrix in Table 2.4 are generated from the 4578 node matrix in Table 2.1. It is not surprising that the multifrontal method is more efficient than traditional LU factorization on these two matrices, since the 9156 node matrix has approximately 12 nonzeros per row and the 4578 node matrix has approximately 22 nonzeros per row. Table 2.5 shows the results for matrices with the sparsity characteristics of those seen in short-term-dynamic-simulation Jacobians. All the matrices in Table 2.5 have approximately 4 to 5 nonzeros per row, which can be considered relatively sparse. As shown in Table 2.5, the traditional LU factorization is superior to the multifrontal method on these short-term dynamic simulation matrices.

2.4.3. Summary of the Results and Remarks

The UMFPACK gains in Table 2.1 to Table 2.5 are plotted vs. the number of nonzeros per row for each matrix in Fig. 2.3. This plot shows that UMFPACK gain is a function of the degree of sparsity. This figure is also consistent with the claims made in the literature about the performance gains obtained with multifrontal methods but shows a well-behaved decrease in multifrontal-method gain with increasing of the level of sparsity.

The relationship between UMFPACK gain, sparsity and sparsity pattern is expected to be complex and is likely the cause of the scatter in the data points in Fig. 2.3. Expecting that UMFPACK gain is affected by the degree of sparsity (number of nonzeros per row) as well as sparsity pattern/topology (very approximately measured by the number of fill-ins), we plotted UMFPACK gain versus number of nonzeros per row in L and U factors in Fig. 2.4.

The scatter in the data points in Fig. 2.4 is significantly less than that in Fig. 2.3, indicating that the UMFPACK gain is affected by both degree and pattern of sparsity.

We wanted to compare our multifrontal gains with those reported in the literature. Those studies have been conducted to determine the performance of different variants of multifrontal methods on matrices with different characteristics. While claims in [17], [71]have been made that multifrontal methods are superior to traditional LU factorization—and we do not dispute these claims for the matrices tested—we found that the metrics used by these authors are not the same ones used in our work and therefore the results are not directly

comparable with ours. In [17], the author compared the performance between different multifrontal variants and supernodal LU factorization variants on symmetric and unsymmetric matrices and concluded that multifrontal methods are superior to supernodal LU factorization. However, the metric used in [17]is the total execution time for processing of the matrix, which included optimal ordering, and the symbolic and numeric phases for each package; the author did not measure and compare the execution time for the numerical factorization phase alone (as is reported here) for each package. Therefore, the results obtained in [17] are not comparable with the ones in this paper. In [71], the author compared the performance between different variants of multifrontal methods and variants of supernodal LU factorization on unsymmetric matrices. However, because most of the matrices that occur in common power system problems are incident symmetric matrices, the test in [71] is not a good indication of the performance of multifrontal methods relative to traditional LU factorization on power-system matrices.

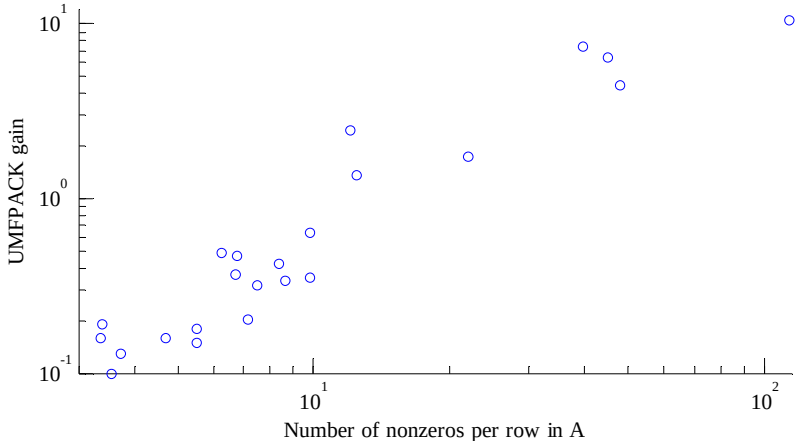

Fig. 2.3 Plot of UMFPACK gain vs. number of nonzeros per row in matrix A for each matrix

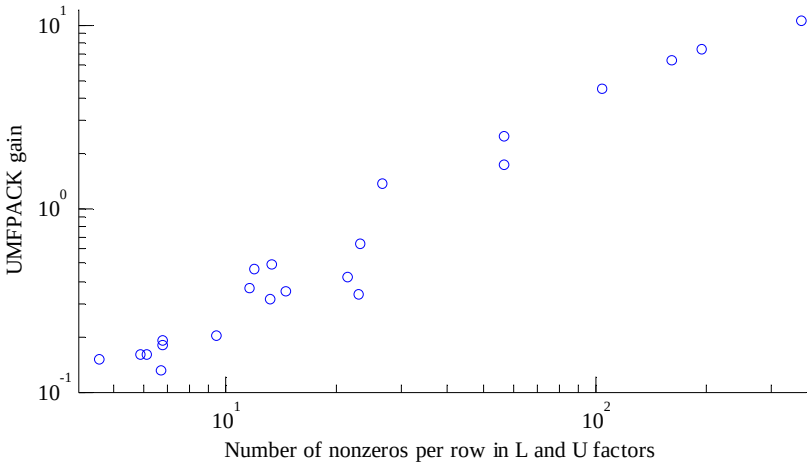

Fig. 2.4 Plot of UMFPACK gain vs. number of nonzeros per row in *L* and *U* factors

Therefore, with no clear evidence existing to the contrary in the literature and given the predictable behavior of the UMFPACK gain relative to traditional LU factorization on the range of matrices studied in this paper, including power-system type matrices, it appears clear that (at minimum) the variant of the multifrontal method implemented by UMFPACK is not competitive with traditional LU factorization of matrices found in common power-system simulation problems.

2.4.4. Conclusions

The execution time of the UMFPACK sparse multifrontal method has been compared to that of traditional LU factorization used for decades by the power industry to solve a variety of sparse matrix equation problems. While it is impossible to perform exhaustive testing, these results demonstrate that the multifrontal method, as implemented by UMFPACK is not competitive in power system applications, except for rare problems where the matrices are abnormally dense. The UMFPACK multifrontal method does become competitive as the

density of the matrices increases. The crossover point occurs when the number of nonzeros per row exceeds approximately 10.

We understand that the applicability of our conclusion is limited in several ways. Our results apply only to the variant of the multifrontal algorithm implemented by UMFPACK, one of the industry's standards. We understand that there are many variants of multifrontal methods and that they are affected by a host of factors pointed out by one of our reviewers: task dependency, numerical factorization implementation, pivoting strategy, variant of BLAS used, and block size to name a few. We have not tested the many possible variants. Also, we have not conducted performance testing on forward and backward substitution. Further our tests were run only on the PC architecture mentioned in the body of the report: no attempt was made to perform a comparison on a vector or parallel processor.

The results suggest that multifrontal methods may not be an effective way to improve the execution time for large system simulations. At minimum, before using any multifrontal variant the programmer/engineer must compare its performance with that of the traditional LU factorization algorithm on matrices that are characteristic of those to which it will be applied.

CHAPTER 3 .

A MODIFIED WARD EQUIVALENT FOR ERCOT SYSTEM

This chapter presents the method used for developing a backbone equivalent for a large-scale power system and then the method is applied to the ERCOT system. Several prevailing network reduction techniques are first reviewed. A brief introduction to ERCOT system is given in this chapter. The equivalents generated are validated using different metrics and promising results are obtained.

3.1 Literature Review on Network Equivalencing Techniques

Depending on the application of the equivalent, the network equivalencing technique can be generally divided into two categories: static and dynamic equivalencing. For dynamic reduction, the focus is to capture the dynamic characteristics of the full system, and the reduced model is intended for system dynamic analysis, such as real-time power system transient stability assessment [41]. For static reduction, the reduced model is intended for static power flow studies, such as online contingency evaluation, market-based system analysis and system-planning studies. Since the focus of this thesis is on system planning, only the static equivalencing technique is reviewed and the term “network reduction” refers only to static power system reduction.

Currently there exist several prevailing classes of equivalents. One of them is the REI (radial equivalent independent) equivalent, which was first proposed in [42] and further discussed in [43] and [44]. The REI equivalent aggregates power and current injections at designated external buses on to a fictitious ‘REI’ node,

and the designated group is then replaced by a fictitious bus in the reduced model. The REI nodes are connected to boundary buses through a radial network called the REI network. The criteria for aggregating buses can be selected based on generation and load conformity, or electrical, geographical, ownership groupings, etc.

REI equivalent may have some limitations. One limitation is that the fictitious 'REI' nodes may suffer from low bus voltage magnitude. To solve this problem, solutions were proposed in [44] to improve the REI equivalent. The performance of the improved REI equivalent was compared against other types of equivalents and promising results were observed.

Another limitation with REI equivalent is that the REI equivalent is operating point dependent: the admittances of the REI network are functions of operating condition at which REI equivalent is constructed. Therefore, as the operating point moves away from the base case, the accuracy of the REI equivalent will in general deteriorate.

The REI equivalent also has the limitation that it lacks the ability to preserve low degree of sparsity of the reduced model. Due to the extra interconnections introduced by REI network, an REI equivalent always tends to be denser than its Ward equivalent counterpart. This limitation decreases the computational efficiency of the REI equivalent, and may limit its applicability in problems where high computational efficiency is required.

Another widely used type of equivalencing method is the Ward equivalencing technique, which was first proposed by Ward in [45] and further discussed in

[46]-[49]. The basic idea of Ward reduction method is to eliminate the buses in the external subsystem through Gaussian elimination, while keeping the internal subsystem intact.

The classic Ward reduction method has two versions [48], differing in the ways that they model bus injection at each node. The first version of classic Ward reduction is referred to as Ward Injection method. In this method, the power injection at each bus is converted to injected current before eliminating the external buses. After the external buses are eliminated, current injection is converted back to power injection at each bus. The second version of classic Ward reduction is referred to as Ward Admittance Method. In this method, power injection at each bus is converted to constant shunt admittance instead of current injection before reduction. The second version is less preferable than the first version, because it may yield unrealistic admittance in the equivalent, and the shunt-admittance modeling of bus injections may not be appropriate for all loads.

The classic Ward equivalent also has its limitations. One such lies in its inability to accurately model the reactive power response from the external buses. In order to overcome this limitation, several modified versions of classic Ward equivalent were discussed in [47]-[52]. In [47], a Ward-PV equivalent was proposed. In this model, all the external PQ buses are eliminated while the external PV buses are retained. However, retaining of all the external PV buses increases the size of the equivalent and thereby decreases the computational efficiency of the equivalent. To further improve the Ward equivalent, an extended Ward equivalent for static security analysis was proposed in [51]. In the extend

Ward equivalent, a fictitious PV bus is attached to each boundary bus. This fictitious PV bus contributes no active power injection but provides adjustable reactive power injection to the system. The reactive power provided by the fictitious is zero under base case and will vary as operating point moves away from base case.

In [53], J. Mochowski et al. proposed a reduced Ward-PV equivalent. In this method, all the external generator nodes are retained and aggregated into several groups. After generator aggregation is done, each group is replaced by an equivalent generator node using Zhukov method [54]. Therefore, the number of nodes retained is reduced. By using the Zhukov method, the dynamic properties of the system can also be maintained, which make the reduced Ward-PV equivalent also applicable in dynamic studies.

Other limitations of the traditional Ward equivalent make its application to the optimal power flow problematic. It is well known that the traditional Ward equivalent may “smear” the injections of external generators over a large number of boundary buses. For system planning studies and market-based analysis, modeling of fractions of generators at different buses is not practical. To overcome this limitation, authors in [55] proposed a “combined” equivalent for the Northeast part of the U. S. power grid. To generate such a “combined” equivalent, the classic Ward Injection Method is first applied to eliminate all external buses except those that are generator buses. Then based on “electrical distance”, external generators are “moved” to the closest retained buses. The Ward reduction is continued to eliminate the external generator buses that have

become vacant. With generators retained as whole, the original generator cost functions can be directly applied and the equivalent can be used in market analysis. However, the internal-system power flows and bus voltages in this equivalent are very different from that in the original system.

In recent years, several network reduction techniques were proposed for system planning and market analysis [56]-[59]. The methods proposed in [57] - [59] are based on dc power flow assumptions and power transfer distribution factors (PTDF). The fundamental concept of these two methods is to aggregate buses while keeping the inter-zonal topology the same as the original (full) system. However, the equivalents generated by these methods contain only equivalent lines with no MVA ratings on them, and currently no existing methods in the literature discusses how the line limits should be assigned for these equivalent lines. Therefore, these two methods may not be applicable in market based analysis where congestion information is required.

3.2 Objective of the Study and Requirements for Equivalent

The objective of this study is to develop a dc backbone equivalent for the entire Electric Reliability Council of Texas (ERCOT) system to be used in a system planning tool for making policy and investment decisions that take into account of the market structure and greenhouse gas (GHG) regulations. A dc rather ac model was chosen for the equivalent because the PF problem becomes linear under dc assumptions and therefore the solution requires much less execution time and convergence is guaranteed. The assumptions used to justify

using any of the various Ward equivalents in traditional applications are violated when applied to developing such a backbone equivalent.

First, in the traditional scenario, the internal area is geographically and electrically localized, and the external area is electrically remote from the internal area. However, in the equivalent to be used in this study, the internal area is neither geographically nor electrically localized. Also, for the external network, most parts of it are not electrically remote from the internal area.

Second, in the traditional scenario, the generators in the external area are either eliminated or replaced by equivalent generators. The injections from external generators are either modeled as small pieces of injections over a large number of buses, or aggregated to equivalent generators. However, for system planning studies to be carried out in this paper, all the generators participate in the market should be retained and each generator should be retained as whole.

Therefore, a novel modified Ward equivalent [60] that can meet these requirements is implemented in this study.

3.3 Brief Introduction to Ward-Type Equivalent

In the Ward (bus elimination) approach, the power system under consideration is usually separated into two parts: the studied system and the external system, as shown in Fig. 3.1. The studied system can be further partitioned into internal buses and boundary buses. The internal buses are interconnected with external system through the boundary buses.

During the reduction process, the external buses are collapsed and the branches are eliminated via partial triangular factorization of the network matrix

and the eliminated branches are replaced by equivalent lines between (collapsed) boundary buses. The electrical power injected at the external buses is first modeled as equivalent current injections at the boundary buses and then converted back to power injections based on the bus voltage at boundary buses. After elimination, the internal system remains unscathed while the external subsystem is eliminated.

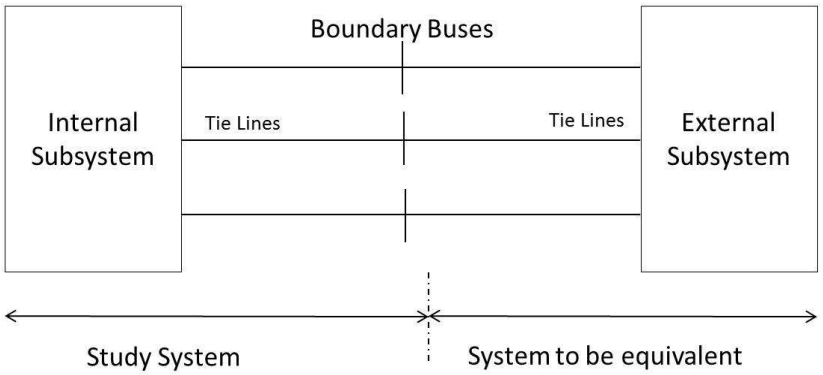

Fig. 3.1 Partitioning of the system

3.4 A Modified Ward Reduction for ERCOT System

3.4.1 Selecting Buses to Retain

The first step in conducting a network reduction is to select the study system. Since the equivalent to be generated will be used to conduct optimal generation investment planning that taking into account of the environmental regulations, it is important that the system congestion information be retained in the reduced system.

The congestion information was obtained from the *ERCOT Planning and Operation Information Database* (the database is proprietary), which includes not only the ERCOT congestion reports from year 2000 to 2008, but also the

transmission planning reports for year 2010 to 2015. These data bases were used to identify congested lines and congested paths, which were retained in the model.

Another criterion for selecting retained buses is the voltage levels of the buses. In general, high-voltage buses are more important to retain since these are the electrical nodes through which bulk power flows. Therefore, besides the congested transmission lines/paths, we experimented with retaining different sets of high-voltage buses using voltage level as the criterion.

3.4.2 Modeling of Special Elements

Specific elements in the system need special handling before the process of network reduction is conducted. In the ERCOT system, the elements need to be handled are HVDC lines. Prior to the process of reduction, each HVDC line in the system is replaced by a pair of generators connected to the "from" and "to" bus as shown in Fig. 3.2. If dc lines and converters are assumed to be lossless, the following relationship can be obtained:

$$p_{ac\_from} = p_{ac\_to} \tag{3.1}$$

and the outputs of the two generators are given by:

$$p'_{ac\_from} = p_{ac\_from} \tag{3.2}$$

$$p'_{ac\_to} = p_{ac\_to} \tag{3.3}$$

where p_{ac_from} and p_{ac_to} are the power injections at the "from" end and "to" end of the HVDC line, and both p_{ac_from} and p_{ac_to} are at the ac side of the converters; P_{Loss} is the power loss on the HVDC line; and p_{dc_from} and p_{dc_to} are the power flow at the dc side of the converters.

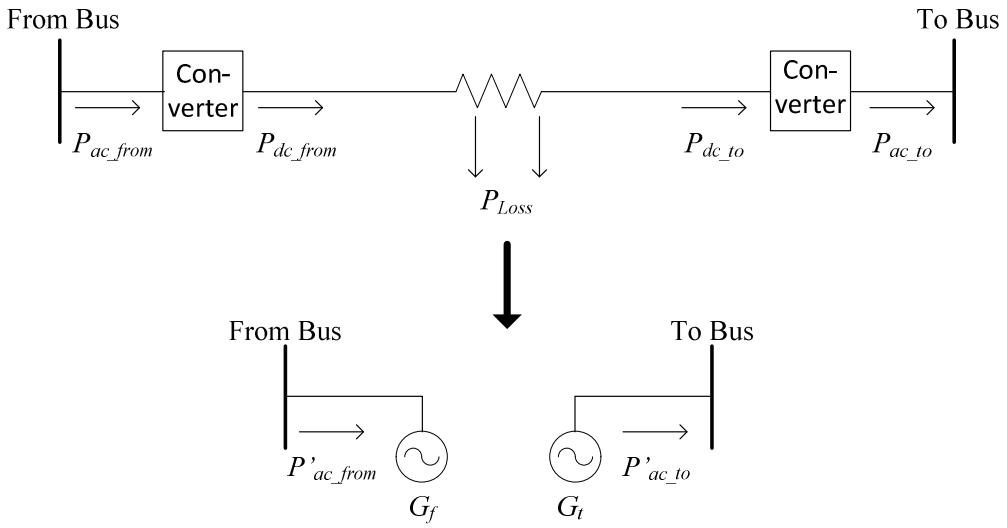

Fig. 3.2 Handling of HVDC lines

After the handling of special elements is completed, a base case can be obtained which will be later used for comparison with reduced models and conducting network reductions.

3.4.3 Eliminating External Subsystem and Moving Generators

After the retained buses are selected, the network reduction proceeds in the following steps. First, the Ward network reduction described in [45]-[48] is applied to the entire ERCOT system to remove all external buses. Since most of the retained lines in the reduced model have impedances smaller than 0.01 p.u., equivalent lines with impedances larger than 5.0 p.u. can be removed in the equivalent without significant degradation of the model.

In the second step, the Ward network reduction is conducted again but with a new set of buses retained: the buses retained in the first step and all the generator buses. This model is referred to as the “reduced model with all generators” and will be used in the next step to determine the movement of external generators.

The third step is to assign external generators to retained buses. To demonstrate the procedure of moving generators, a small portion of the reduced model with all generators is shown in Fig. 3.3. As shown in Fig. 3.3, generators *G1* and *G2* are connected to internal system through multiple paths. For example, *G1* is connected to internal buses through transmission line 1-3, transmission line 1-4, or the combination of transmission line 1-2 and 2-5, etc. It should be noted that the actual reduced model with all generators is much more complicated than what is illustrated in Fig. 3.3.

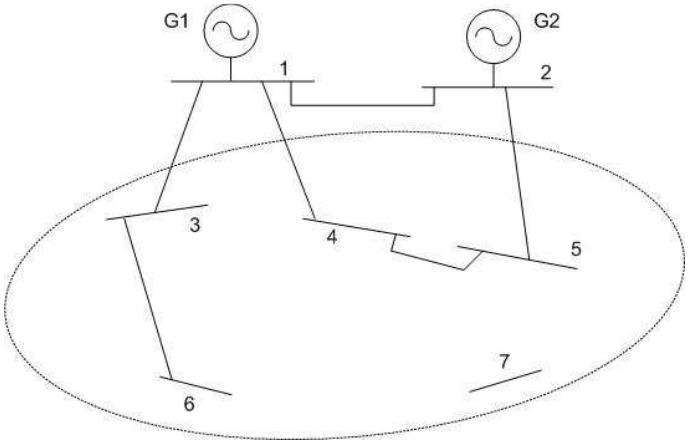

Fig. 3.3 Reduced generator model with all generators

The electrical distance between two buses *A* and *B* is defined as

$$Dis_{AB} = \min_{k\in\{k_1 \ldots k_n\}} \left(\sum_{k_i=1}^{k_i=m} \sqrt{r_{k_i}^2 + x_{k_i}^2} \right) \tag{3.4}$$

where m is the number of transmission lines that connected bus *A* and *B* in path k_i, and n is the number of paths that between bus *A* and *B*.

Assume the transmission lines that connected generator *G1* to the internal buses in Fig. 3.3 have the impedances listed in Table 3.1

TABLE 3.1
IMPEDANCE OF TRANSMISSION LINES IN FIG. 3.3

Transmission Line	$\sqrt{r^2 + x^2}$ (p.u.)
1-2	0.01
1-3	0.02
1-4	0.01
2-4	0.02
2-5	0.01
3-6	0.015
4-5	0.04

Based on (3.4), the electrical distance between generator *G1* and internal buses can be calculated as

$$Dis_{G1-3} = 0.02$$

$$Dis_{G1-4} = \min\{0.01, 0.06\} = 0.01$$

$$Dis_{G1-5} = \min\{0.05, 0.02\} = 0.02$$

$$Dis_{G1-6} = 0.035$$

From the above calculations, generator *G1* is electrically closest to bus *#4* and should be moved to bus *#4*. Following the similar approach, all the generators in the system can be moved to their electrically closest buses. After the movement of the external generators is determined, the external generators are attached to their corresponding internal/boundary buses in the equivalent produced in step one.

In the equivalent model, generators' real power limits remain the same as in the full system. Since the equivalent is intended to be used with system planning tools for dc OPF based studies, the reactive power limits will play no role in the solution process.

3.4.4 Moving Load

In the classical Ward equivalent, the retained-line flows are exactly the same as the corresponding lines in the full model. This is achieved by breaking-up each external generator and load into multiple fractions with each fraction moved to a different boundary bus. However, in the modified Ward equivalent used here, each generator is moved integrally to a retained bus. To maintain the retained-line flows the same as those in the full model, a procedure called the "inverse power flow" is designed to compensate the movement of generators.

The objective of the inverse power flow program is to move the load in the system so that the retained-line MW flows in the reduced system exactly match those in the full system. It is assumed in the "inverse power flow" program that the bus voltage angles in the reduced model are the same as those at the corresponding buses in the full system.

The inverse power flow program proceeds in the following steps. First, the admittance matrix Y is constructed based on the equivalent network model. In the second step, the power injection at each bus in the reduced system is calculated by using the Y matrix and bus voltage angle vector. Once the power injection at each bus is obtained, the nodal power injection is used to determine the amount of load assigned to each bus based on the existing generation at each bus. By using this

approach, the flows on retained lines match exactly those on the corresponding lines in the full model. And the sum of load added at each bus in the equivalent equals the total load in the original system.

3.4.5 Introduction to the ERCOT System

Fig. 3.4 shows the one-line diagram of the ERCOT system, which contains 6072 buses, 687 generators, 7504 branches, and 3 HVDC lines. The lines shown in Fig. 3.4 are transmission lines whose voltage levels range from 69 kV to 345 kV. The total generation and load for the 2011 summer-peak case are 72826 MW and 71204 MW, respectively, with a loss of 2.22% (of the total generation).

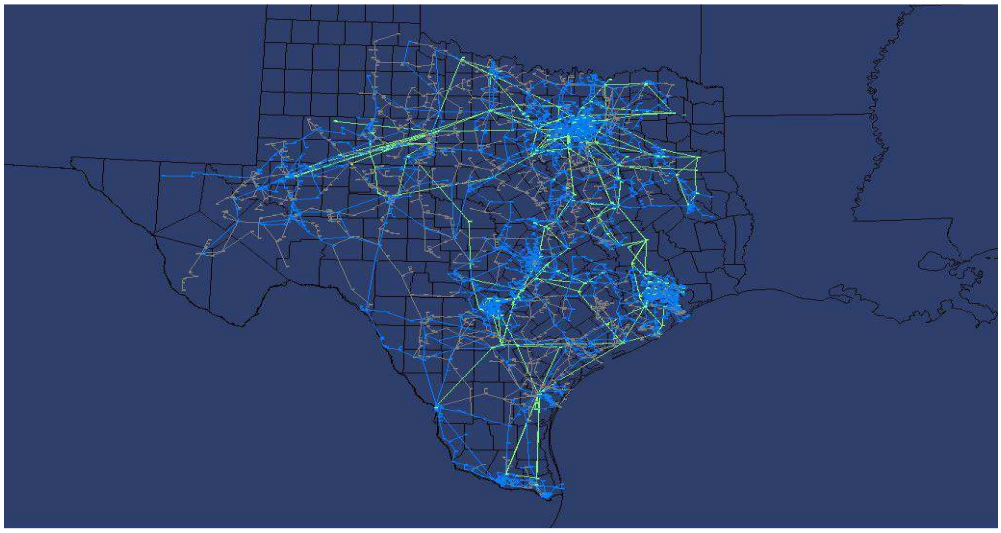

Fig. 3.4 One-line diagram of the full ERCOT system

3.4.6 279-Bus Equivalent of ERCOT

Following the procedure described above, a 279-bus dc equivalent (shown in Fig. 3.5) of the ERCOT system is first produced. In this equivalent, all the 230 kV-and-above buses are retained, which means all 230 kV-and-above congested lines/paths are retained, while congested lines/paths operating at less than 230 kV

are ignored. In particular, this equivalent model consists of 1279 TLs, among which 414 lines are physical lines while the remaining 865 lines are equivalent/fictitious TLs generated in the reduction process.

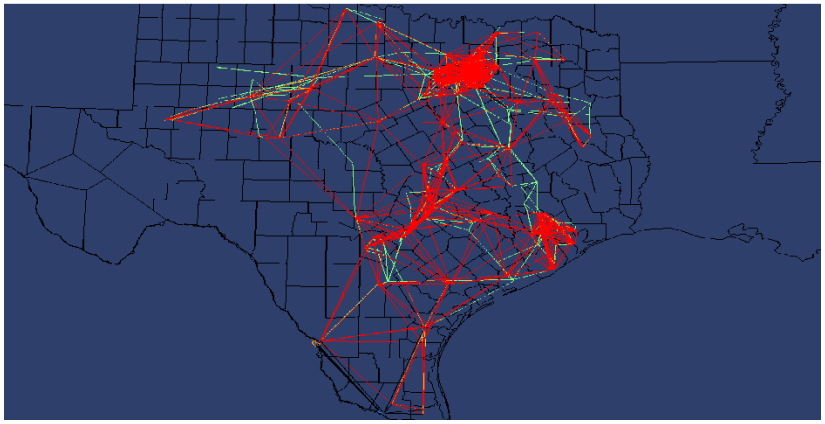

Fig. 3.5 One-line diagram of the 279-bus reduced model

CHAPTER 4 .

VALIDATION OF THE REDUCED MODEL

In this chapter, the accuracy of the equivalent generated in chapter 3 is evaluated. Metrics are developed to evaluate the error between the equivalent and full model under the base case and the changed generation case. Conflicts between accuracy and size exist when generating equivalents: generating a small equivalent sacrifices accuracy; generating a large equivalent gains accuracy but sacrifices computational efficiency. To study the relationship between the accuracy and size of an equivalent, several equivalents were generated and their accuracy was tested and compared. The performance of the equivalent was also tested in terms of dc optimal power flow.

4.1 Evaluation of the Reduced Model in Terms of Power Flow Solutions

In the base case, the power flows (PFs) on the retained lines of the equivalent exactly match those in the full model. For changed cases this is not true. As the operating point is moved away from the base case, e.g., the generator power orders in the reduced models are changed, it is necessary to quantify the difference between the full and the reduced models. The test to examine the changed dispatch involves decreasing the coal generation by increasing amounts and then picking up the decrease with increases in power orders to the natural-gas units. This test is simulates, in an approximate way, the potential generation-mix changes under environmental regulations. It is likely that under CO_2 cap-and-trade schemes that coal-fired generation will be reduced at times when CO_2

emissions threaten the cap and the system will thus require a concomitant increase in gas fired generation. In this subsection, the 279-bus equivalent generated in chapter 3 CHAPTER 3 is used to evaluate the performance of the equivalent.

Several metrics are used to determine the accuracy of the model for changed cases. One is the magnitude of the retained-line-flow errors, i.e., difference between line flows (in MW) calculated using the full and the reduced equivalent models. The second one is the error of these line flows in percentage based on the corresponding lines' MVA ratings. These two metrics are shown in (4.1) and (4.2).

$$Error_i = \left| Pf_i^{full} - Pf_i^{reduced} \right| \tag{4.1}$$

$$Error_i\% = \frac{\left| Pf_i^{full} - Pf_i^{reduced} \right|}{(Lim_{MVA})_i} \tag{4.2}$$

where Pf_i^{full} and $Pf_i^{reduced}$ represent the PFs on retained line *i* from the full model and the reduced model, respectively; the variable $(Lim_{MVA})_i$ is the MVA rating of the retained line *i*.

Another metric used is the average error in the retained-line flows in MW, which is calculated by (4.3).

$$Error_{Avg} = \frac{\sum_{i=1}^{N} \left| Pf_i^{full} - Pf_i^{reduced} \right|}{N_r} \tag{4.3}$$

where N_r is the number of retained lines.

Generators in ERCOT are summarized in terms of fuel types in Table 4.1 (based on the 2011 summer peak case). It is shown in the Table 4.1 that the coal

generation contributes 27.4% and the natural gas generation contributes 62.5% to the total MW generation in the ERCOT.

TABLE 4.1.
GENERATOR INFORMATION IN ERCOT SYSTEM

Gen Fuel Type	Num. of Gens	Generation (MW)
Coal	41	19,961.3
Distillate Fuel Oil (Diesel, FO1, FO2, FO4)	2	0
Hydro	27	0
Natural Gas	477	45,535.0
Nuclear	4	5,131.0
Wind	107	1552.9
Wood or Wood Waste	2	50.0
Waste Heat	2	29.0
Other/Unknown	25	567.6
TOTAL	687	72826.8

The aforementioned test is conducted using the following steps. First, the coal generation is decreased by 1.0%, which is 199.6MW. Then, to compensate the decrease in coal generation, the natural gas generation is increased by 199.6MW, which corresponds to 0.44% of the total generation of natural gas. After the generation of coal and natural gas are changed, the dc power flow is solved for both the full and reduced model. Then the line flows on the retained transmission lines in the equivalent are compared against the same flow in the full model.

Taking the MW flow on the retained lines in the full model as the reference, errors in retained-line flows are calculated with their absolute values plotted in Fig. 4.1 versus retain branch/line ID's whose values were assigned arbitrarily, but contiguously. These errors, in percentage of the corresponding lines' MVA ratings, are shown in Fig. 4.2.

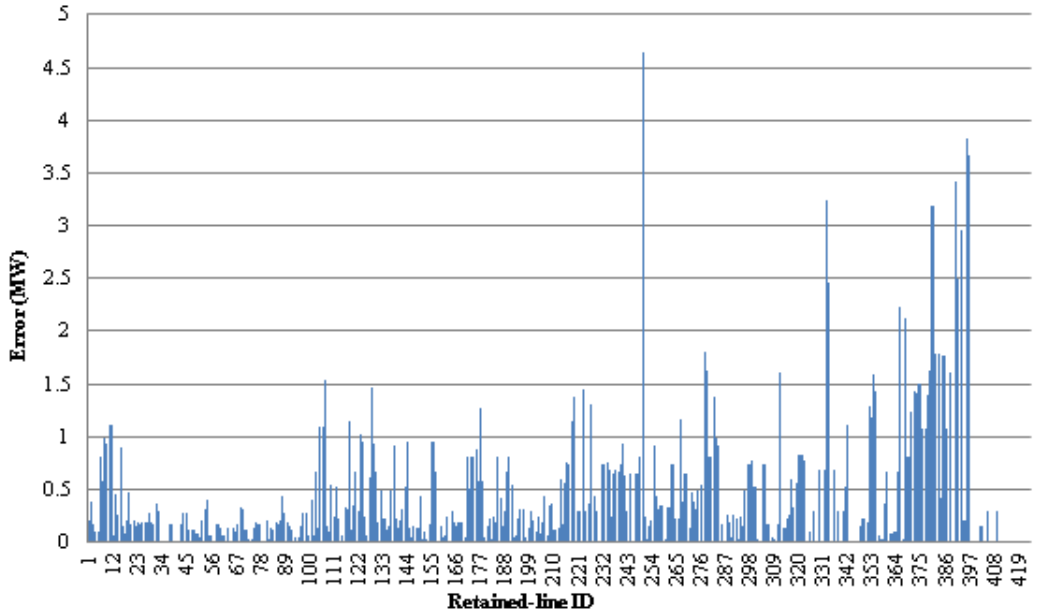

Fig. 4.1 Retained line flow errors in MW

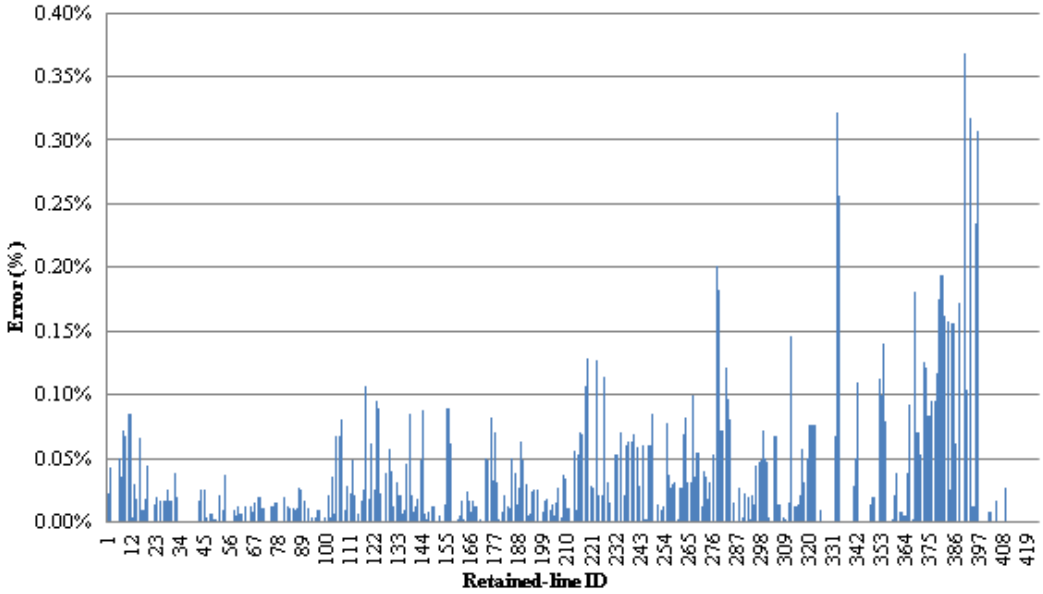

Fig. 4.2 Retained-line flow errors in percentage

From Fig. 4.1 and Fig. 4.2, it can be seen that, when the coal generation is decreased by 1%, the largest error in the retained-line flows is around 4.6 MW, or 0.36% of the corresponding line rating. Most of the errors are smaller than 2.5

MW with only a few lying between 2.5 MW and 4 MW, or between 0.15% and 0.35% of the line rating.

For this 279-bus equivalent, the average error in the retained-line flows is 0.45 MW for a 1% decrease in coal. As we further decrease the coal generation (while increasing the gas generation) the average errors on the retained-line flows are depicted in Fig. 4.3.

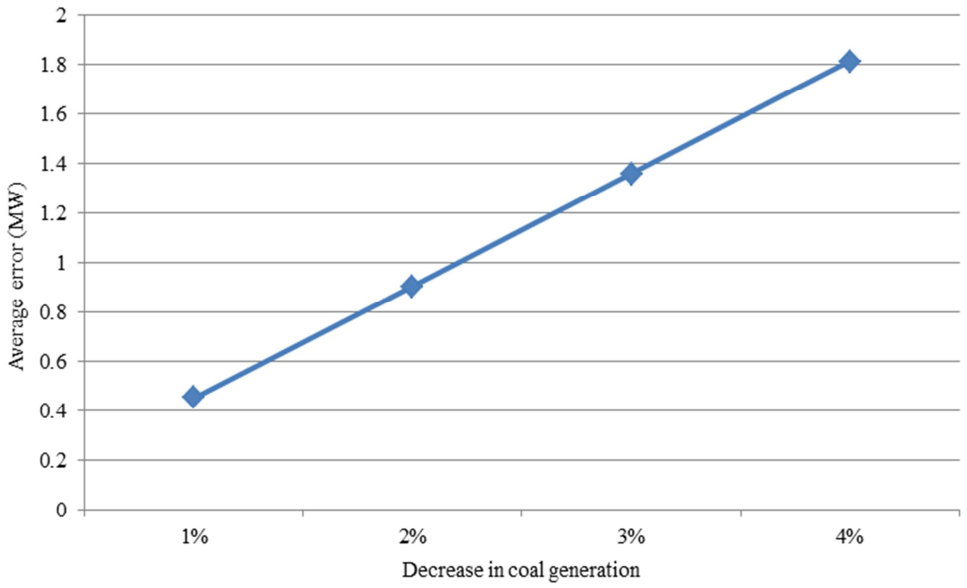

Fig. 4.3 Average errors (MW) in retained-line flows vs. decrease (%) in coal generation

As Fig. 4.3 shows, a 4% decrease in the coal generation will result in an average error of 1.8MW in the retained-line flows.

Intuition suggests that the accuracy of an equivalent is related to its size: the more buses the equivalent retains, the more accurate the equivalent is; however, increasing the size of the equivalent will increase the computational burden. Balancing these conflicting criteria requires engineering judgment. To study the

relationship between size and accuracy, two larger equivalents were generated for the ERCOT system:

- 424 bus model: retain all 138 kV and above congested lines/paths plus 230 kV and above buses.
- 1036 bus model: retain all 138 kV and above congested lines/paths, all the 230 kV and above buses, and all the generator buses.

The schematics of the two equivalents are shown in Fig. 4.4 (a) and (b). The red and yellow lines in these figures represent equivalent lines while other colors represent physical lines.

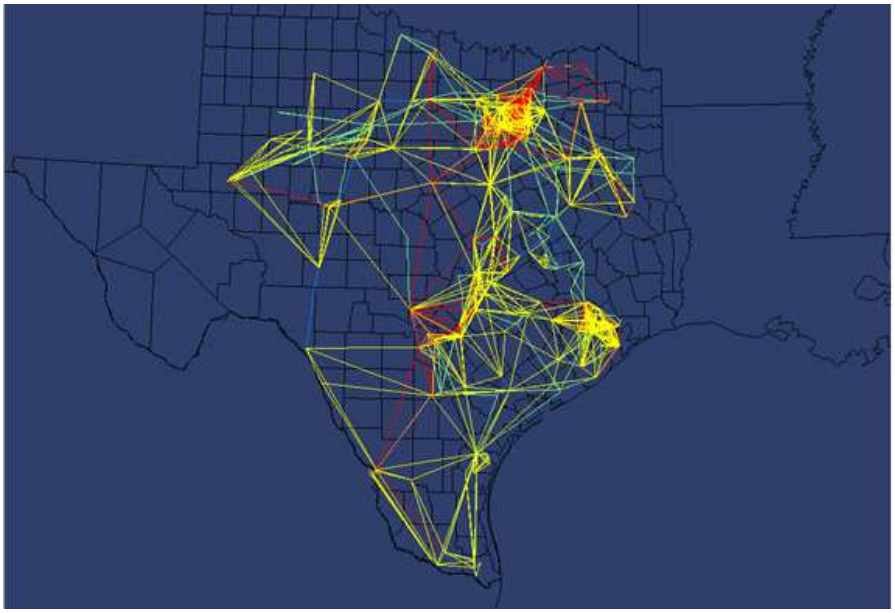

(a) 424-bus equivalent

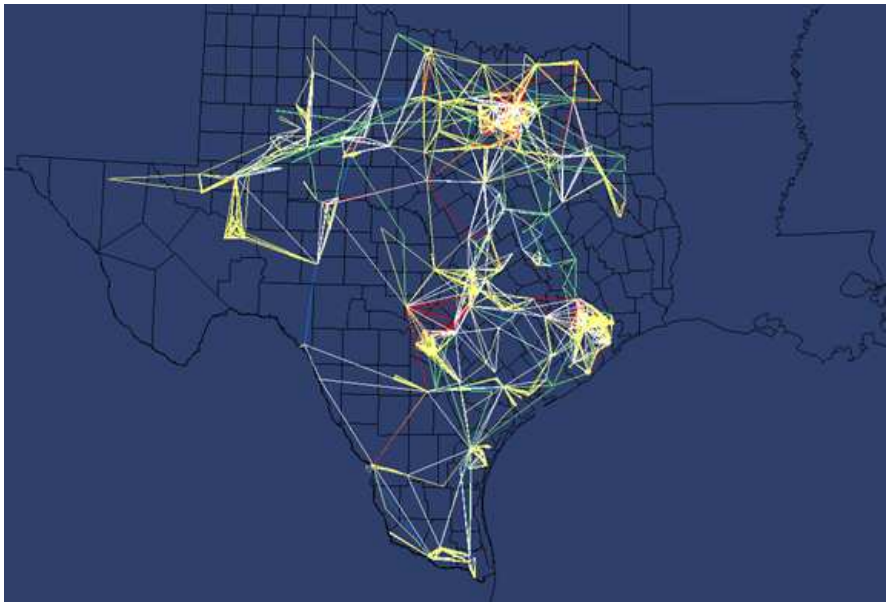

(b) 1036-bus equivalent

Fig. 4.4 Schematics of ERCOT equivalents

The same sets of tests described above are conducted using these two equivalents and the average errors on the retained-line flows are plotted versus coal reduction as shown in Fig. 4.5.

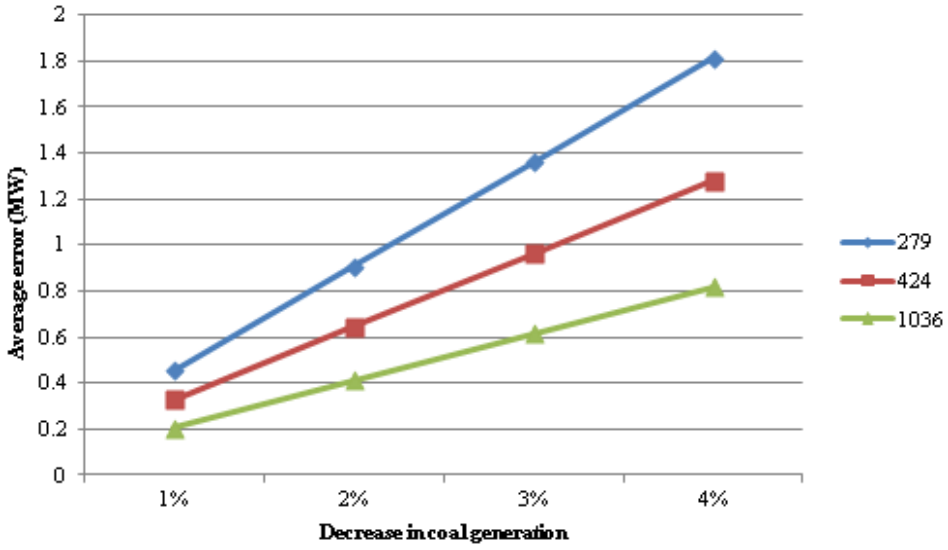

Fig. 4.5 Average errors (MW) in line flows for ERCOT equivalents

As shown in Fig. 4.5, for the 1036-bus equivalent, when coal generation is reduced by 4%, the average error in the retained-line flows is very small, 0.8 MW. And for the 424-bus and 279-bus equivalents, this error increases to 1.3 MW and 1.8 MW, respectively, still well within the range of acceptability. This pattern of increasing error with reduction in number of retained buses is consistent with intuition and is used as a sanity check. Furthermore, the effectiveness of the proposed network reduction scheme is validated in terms of the line-flow metrics associated with power flow solutions under changed dispatches.

In OPF studies, a metric that takes into account maximum line-flow ratings, which are more critical to LMP calculations, is an important criterion. This is addressed in the next section.

4.2 Evaluation of the Reduced Model in Terms of Optimal Power Flow Solutions

Ultimately, the equivalents generated are to be used in OPF studies. Two metrics useful in comparing the accuracy of the full and equivalent models' OPF solutions are the total operating cost difference (error) and average difference in the LMP's, both of which include the effects of constrained lines/paths.

In addition to the network data, generator cost functions were needed and obtained to perform an OPF solution. Since the equivalent will also be used in optimal generation investment studies in which the real-load data are used, it is important to use the real load data rather than the modeled data in the OPF solution comparison. Therefore, the load in the aforementioned ERCOT database is scaled based on the hourly load data obtained from *ERCOT Hourly Load Data Archives* [61]. Solutions from OPF executions using both the equivalent dc model

and the full dc model were obtained and the two solutions were compared. One important metric, and the impetus for creating an equivalent, is the OPF execution time. For the 424 bus equivalent, the dc OPF converged about 6 times faster than when using the full model. The total operating costs, and average LMPs from the two dc OPF solutions for the 424-bus and full models are listed in the second and third columns of Table 4.2, while the corresponding error metrics are shown in the fourth and fifth columns. The test was conducted in Matpower [62]with the Mosek [63] default LP solver.

TABLE 4.2
COMPARISON BETWEEN THE DC OPF SOLUTIONS OF THE FULL AND 424-BUS-EQUIVALENT ERCOT MODELS

	Full Model	424-bus Equivalent	|Errors| (MW)	|Errors| (%)	Standard Deviation (MW)
Convergence	Y	Y	NA	NA	NA
Total Cost ($/Hour)	1,363,111	1,360,559	2552	0.19%	NA
Average LMP ($/MWh)	25.6163	25.6337	0.4621	1.8%	1.952

TABLE 4.3
COMPARISON OF THE GENERATOR DISPATCH BETWEEN THE FULL AND 424-BUS-EQUIVALENT MODELS BASED ON A DC OPF SOLUTIONS

Fuel Type	Equivalent (MW)	Full System (MW)	|Errors| (MW)	|Errors| (%)
nuclear	5131	5131	0.0	0.0%
coal	19576	19577	1.0	0.005%
natural gas	26041	25952	89.0	0.342%
wind	9380	9468	88.0	0.949%
Distillate Fuel Oil (Diesel,FO1,FO2,FO4)	-2	-2	0.0	0.000%
hydro	0	0	0.0	0.000%
waste heat	14	14	0.0	0.000%
wood or wood waste	50	50	0.0	0.000%
unknown	568	568	0.0	0.000%

From Table 4.2, it can be seen that the error in the total operating costs between the two models is 0.19% of the total operating cost. The average LMPs differed by 0.0174 $/MWh, which corresponds to an error of 0.068%.

Another metric used to compare the dc OPF solutions of the full model and 424-bus equivalent is the generator dispatches by fuel type. Generator dispatches and differences (errors) in dispatches are shown in Table 4.3.

It can be seen from Table 4.3 that except for natural gas and wind generators, all the other fuel types have essentially the same total dispatch in the full and equivalent models. The error in dispatch for the natural gas generators is 0.342% of the total natural gas generation. The error in the wind generator dispatches is 0.949% of the total wind generation, values well within the bound of acceptability.

To sum up, the simulation results shown in this section support the conclusion that the 424-bus equivalent is acceptable for dc OPF studies.

4.3 Evaluation of the Reduced Model in Terms of Accuracy of the dc Power Flow Formulation

The previous two subsections have quantified the errors between the dc PF and dc OPF solutions of the full and equivalent ERCOT models. However, dc PF models are inherently approximate and their accuracies are system and case dependent [64]. Before applying the dc equivalent to simulations like a system planning study, it is important to quantify the differences between the power flow solutions for the dc reduced model and the ac full model. In this subsection, the focus is on examining the accuracy of the dc PF formulations for the equivalent model. In order to improve the accuracy of the dc PF formulations for the equivalent, this subsection also examines the influence of loss compensation on the accuracy of the dc power flow model.

4.3.1 Review of Classic dc Power Flow Model

The derivation of dc power flow formulation starts from the ac power flow equations. For the transmission line model shown in Fig. 4.6, the power flow at bus *i* is calculated as

$$\begin{aligned} P_i &= \mathrm{Re}\left\{\vec{V}_i \cdot \vec{I}_{ij}^{\,*}\right\} \\ &= \mathrm{Re}\left\{v_i\angle\theta_i \cdot \left[(g_{ij} + jb_{ij}) \cdot (v_i\angle\theta_i - v_j\angle\theta_j)\right]^*\right\} \\ &= g_{ij}v_i^2 - g_{ij}v_iv_j\cos\theta_{ij} - b_{ij}v_iv_j\sin\theta_{ij} \end{aligned} \tag{4.4}$$

where $\theta_{ij} = \theta_i - \theta_j$, and θ_{ij} is the voltage angle difference across the branch.

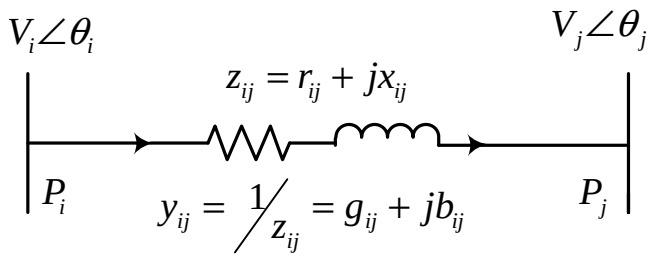

Fig. 4.6 A typical transmission line model connecting bus *i* and bus *j*

In a classic dc power flow model, the following assumptions are made:

- Branch resistance *r* is negligible, and the system is assumed to be a lossless system.

$$r_{ij} \approx 0 \quad \text{so that} \quad \mathrm{P}_{ij} = v_i v_j \sin\theta_{ij} / x_{ij} \tag{4.5}$$

- All bus voltage magnitudes are assumed to be close to 1 p.u.

$$v_i \approx 1, v_j \approx 1 \quad \text{so that} \quad \mathrm{P}_{ij} = \sin\theta_{ij} / x_{ij} \tag{4.6}$$

- The voltage angle difference θ_{ij} across the branches is very small:

$$\theta_{ij} \approx 0, \sin\theta_{ij} \approx \theta_i - \theta_j \quad \text{so that} \quad \mathrm{P}_{ij} = \theta_{ij} / x_{ij} = (\theta_i - \theta_j) / x_{ij} \tag{4.7}$$

Given the above assumptions, the loss in the original ac system is neglected and therefore this model is a state-independent model.

4.3.2 Evaluation of the Accuracy of Classic dc Power Flow Model

An ac PF solution is first solved for the full ERCOT system under the base case. Based on the formulations of the classic dc power-flow model, a dc model for the full ERCOT system is obtained. Automatic generation control (AGC), LTC transformer control and phase shifter control have been disabled when solving the dc PF for the full mode. Once the dc base case is obtained, the modified Ward equivalencing technique is applied to the entire ERCOT system to generate a 424-

bus dc equivalent. Power flows on the retained lines in the equivalent are compared with those on the corresponding lines in the full ac model to measure the errors between dc equivalent and ac full model.

Following the test described in [64], the following criteria are applied when determining the branch-flow errors between the dc equivalent and ac full model:

- All lines that have no MVA rating are neglected.
- All branches that are 100kV and below are neglected. It is assumed that the power flow violations on transmission lines that are 100kV and below can be corrected through long-term system planning.
- All lines that are loaded under 40% of the MVA rating are neglected. Because the equivalent will be used in system planning studies where congested lines play a significant role, lines that are more likely to be congested and can substantially affect the dispatch and pricing are of more interest.

Metrics defined in (4.1) and (4.2) are used to quantify the difference (errors) between the branch MW-flows in the dc equivalent and ac full (unreduced) model. Taking the MW flow on the retained lines in the full ac model as the reference, errors in retained-line MW flows between the full ac model and reduced dc model are plotted in Fig. 4.7 versus retained branch ID. These errors, in percentage of the corresponding lines' MVA ratings, are shown in Fig. 4.8.

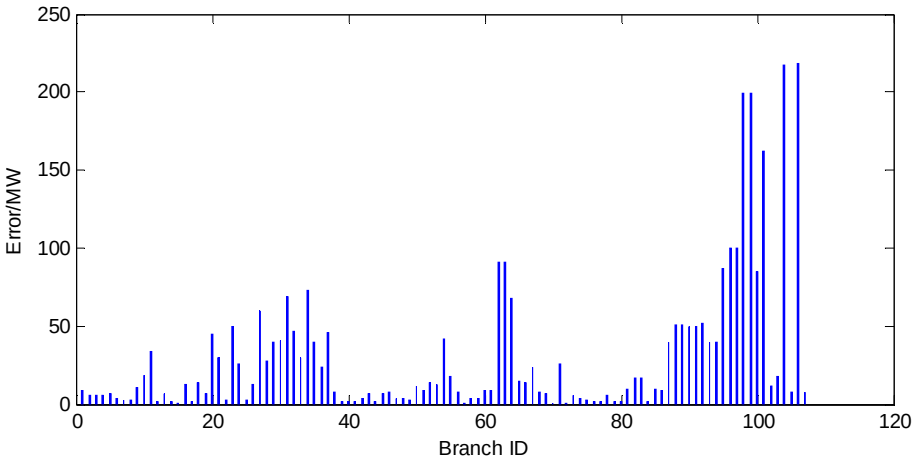

Fig. 4.7 Power flow errors in MW between the reduced dc model and full ac model using classic dc power-flow model

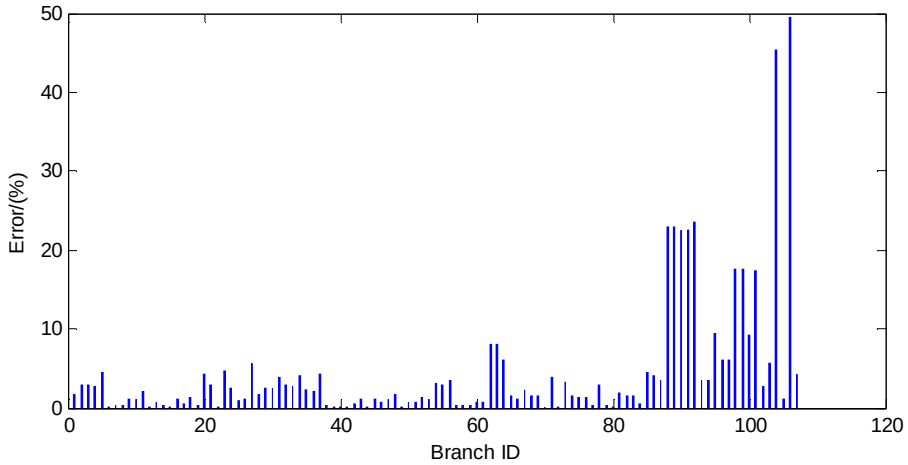

Fig. 4.8 Power flow errors in percentage between the reduced dc model and full ac model using classic dc power-flow model

As shown in Fig. 4.7 and Fig. 4.8, the maximum MW error occurs in branch PFs is about 210 MW, or 50% of the corresponding line's MVA rating. These large branch MW-flow errors are found to occur on the lines that are located near the system slack bus. This observation is expected since all the losses are neglected in the classic dc power-flow model. With the absence of losses in the dc model, the reduction in total generation must be compensated by reduced

generation at the slack bus, a reduction that can become considerable for large systems. Therefore, the branch flows near the slack bus are radically changed because of this reduced generation.

From Fig. 4.7 and Fig. 4.8, it can be seen that about half of the MW errors are above 50 MW, or 5% of the line MVA ratings. Using the metric described in (4.3), the average MW error in branch flows is calculated to be 29.9 MW, which is a relative large error.

The above observances indicate that even in the base case, the errors between the dc equivalent and the full ac model is considerable. As the operating point of the reduced model moves away, this error is expected to increase. The large error with the classic dc power-flow model is not acceptable. To reduce this error, we examined another type of dc power-flow model: dc power-flow model with loss compensation.

4.3.3 Review of dc Power Flow Model with Zonal Loss Compensation and Evaluation of its Accuracy

In this model, the network-modeling assumptions used are the same as those used in the classic dc power-flow model. The difference between the two models lies in the fact that loss is compensated in this model but neglected in the classic model. Loss compensation is done by applying a different multiplier to the load in each zone in the system. With the modeling of the losses in the model, the dc power flow model with zonal loss compensation is a state-dependent model.

The multiplier λ_i used for the load in zone *i* is calculated as:

$$\lambda_i = 1 + \frac{\sum_i P_{Loss}}{\sum_i P_{Load}} \tag{4.8}$$

where $\sum_i P_{Loss}$ is the total loss in zone *i* and $\sum_i P_{Load}$ is the total load in zone *i*.

Following the same criteria described in the previous subsection, errors in branch MW-flow on the retained lines between the reduced dc model and full ac model are plotted in Fig. 4.9. The errors in percentage of the corresponding lines' MVA rating are shown in Fig. 4.10.

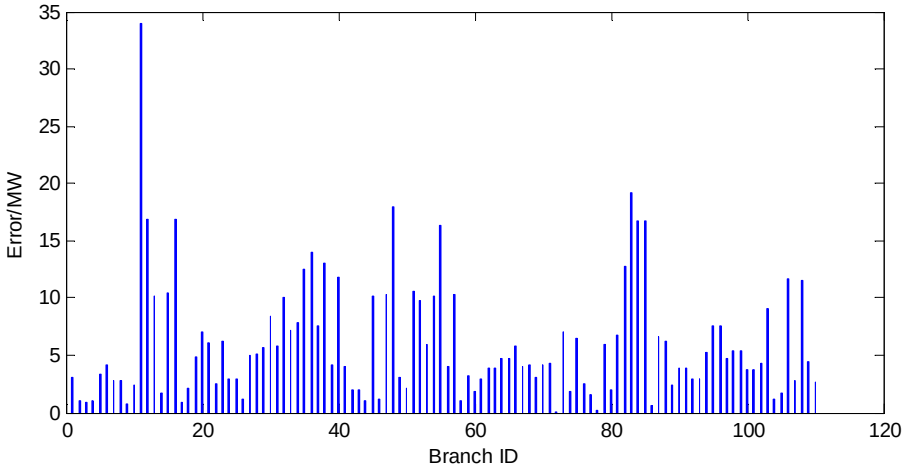

Fig. 4.9 Differences between branch MW-flow on the full ac model and reduced dc model with zonal loss compensation

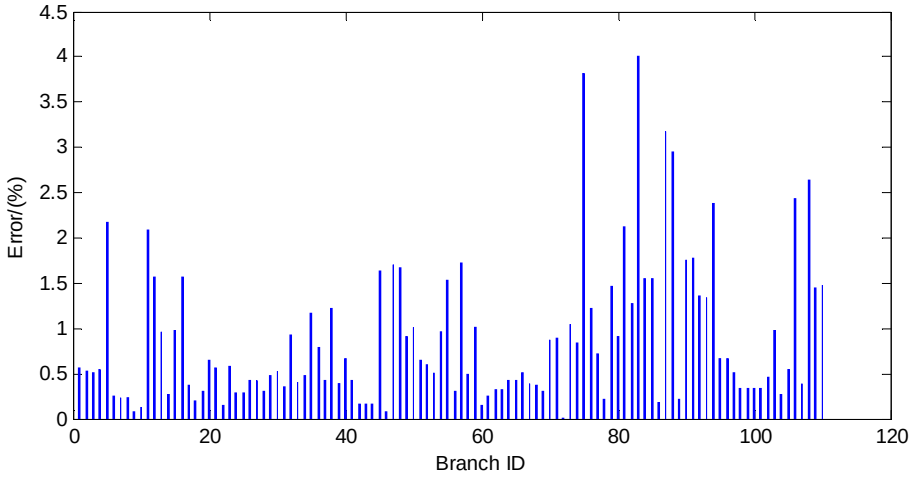

Fig. 4.10 Branch MW-flow errors in percentage of the reduced dc model with zonal loss compensation

Fig. 4.9 and Fig. 4.10 show that most of the errors are well below 15 MW, or 2.5% of the corresponding line's MVA rating. Only a few errors range from 15 MW to 33 MW, or 2% to 4% in terms of corresponding lines' MVA rating. The maximum error occurs in dc power-flow model with loss compensation is around 34 MW, or 4% of MVA rating of the corresponding lines, which is much smaller than the maximum line-flow error in classic dc power flow model. Not unexpectedly, this large error occurs on a line which has a large MVAR flow in the ac model.

The average error in the dc power-flow model with zonal loss compensation is calculated to be 6.0 MW, which is around 1/5 of the average error in the classic dc power-flow model.

4.3.4 Conclusions

The above results show that both the maximum error and average error in the dc power flow model with zonal loss compensation are much smaller than the ones in the classic model, which suggests that the dc power-flow model with zonal loss compensation is superior to the classic dc power-flow model. The dc power flow model with zonal loss compensation takes into account the losses in system, which is a state-dependent model. Given a solved ac solution, the dc power-flow model with zonal loss compensation yields reasonable accuracy. For classic dc power flow model, even though it is state-independent and is easy to construct, the result show that using this model for large-scale power system, such as the ERCOT system, can yield significant errors in branch flow. Therefore, the dc PF model with zonal loss compensation is chosen to be implemented in the following optimal generation investment study.

CHAPTER 5 .

APPLICATION OF THE EQUIVALENT IN SYSTEM PLANNING

In this chapter, the 279-bus equivalent is used in SuperOPF Planning Tool to determine optimal generation planning in the ERCOT system. A brief introduction to the structure and formulation of the SuperOPF Planning Tool is presented. Modeling of the data and description of the cases are provided. The results are analyzed and conclusions are drawn.

5.1 Introduction to the SuperOPF Planning Tool

The SuperOPF Investment Planning Tool, developed by Cornell, is a package whose major function is to optimize generation investment and retirement while maintaining system reliability and accounting for various system constraints such as generation building limits and environmental regulations.

Using the 279-bus ERCOT equivalent yields large execution-time savings when used in the SuperOPF environment. On a state-of-the-art PC, it takes the SuperOPF less than 15 minutes of execution time with the 279-bus equivalent, while solving the same problem with the full ERCOT model takes more than 24 hours.

The formulation of the optimal generation investment problem in the SuperOPF is presented as shown in (5.1). The detail information about the SuperOPF is of less interest in this report and therefore not presented. Detail information regarding the explanation of the formulation, as well as structure and application of the SuperOPF planning tool can be obtained in [5] and [28].

$$\max_{p_{ijk}, I_{ijk}, R_{ij}} \left\{ \sum_i \sum_j \begin{bmatrix} (\sum_k H_k (B_{jk} - (c_i^F + a_{jk} e_i) p_{ijk})) \\ -(c_i^T (p_{ij}^0 + I_{ij} - R_{ij}) + c_i^I I_{ij}) \end{bmatrix} \right\} \tag{5.1}$$

subject to

$$p_{ij}^0 + I_{ij} - R_{ij} \geq p_{ijk}$$
$$p_{ijk} \geq \alpha_i^{\min} (p_{ij}^0 + I_{ij} - R_{ij})$$
$$K_{ij} > I_{ij}$$
$$\sum_j L_{jk} = \sum_i \sum_j p_{ijk}$$
DC network constraints

where the following notation is used:

a_{jk}: emission cost vector at node j in hour k, \$/tonne

B_{jk}: benefit function for demand response

c^F_i: cost of fuel, operations and maintenance per MWh

c^I_i: annualized cost of new investment

c^T_i: cost of taxes and insurance per MW

e_i: emissions vector for generation type i, tonnes/MWh

i: generator index

H_k: number of hours that system is at load profile k

I_{ij}: capacity investment

j: node index

k: representative hour index

K_{ij}: max investment in fuel type i at node j

L_{jk}: net load

p_{ijk}: aggregate real power output from generator i at node j during representative hour k

p^0_{ij}: existing generator capacity

R_{ij}: capacity requirement

α_i^{min}: minimum generation for type i

5.2 Data Preparation

The SuperOPF optimizes generation investment and retirement across multiple load scenarios. In this study, twelve different load scenarios are modeled, each of which corresponds to a different hour type during a year. Load is scaled in each representative hour type and the load scaling factors are calculated based on the load profile obtained from the *ERCOT Hourly Load Data Archives* [61]. Each season consists of four types of hours: peak, high, medium and low. Since the load profile in spring and fall are very similar, spring and fall are combined together as one season referred to as “Fall & Spring” in the model. The summer representative hours make up the greatest portion of the year: May through September. The winter hours comprise three months: December, January and February, with the remaining three months falling into the “Fall & Spring” category. The frequency of each representative hour type and the scaling of load in each representative hour type are shown in Fig. 5.1 and Fig. 5.2. In order to account for reliability, a 10% reserve requirement is added to the system. To

represent unit availability, generator contingencies are included in the model. This is done by de-rating a generator's maximum output capacity in each season, with each generation type de-rated by a different percentage [65].

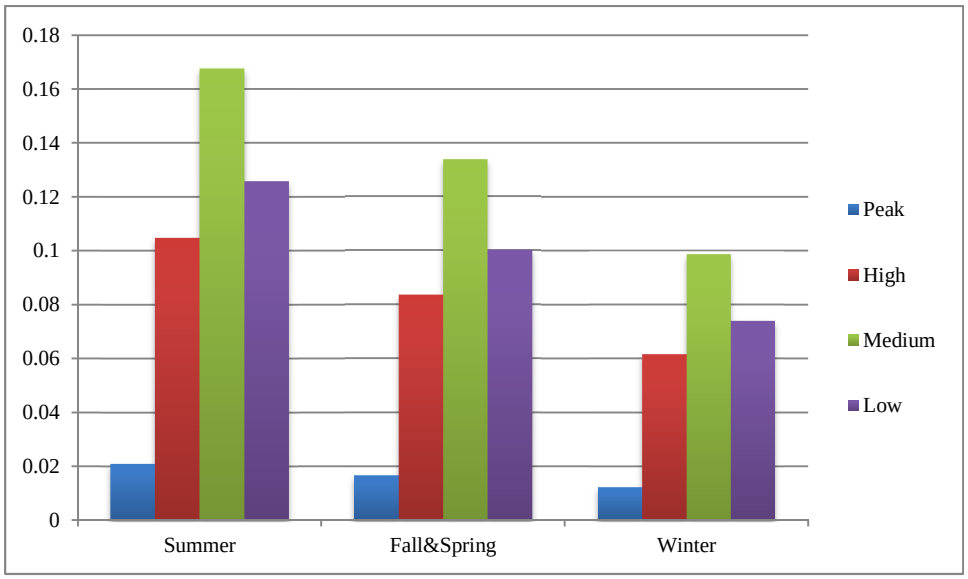

Fig. 5.1 Relative Frequency of Representative Hour Types

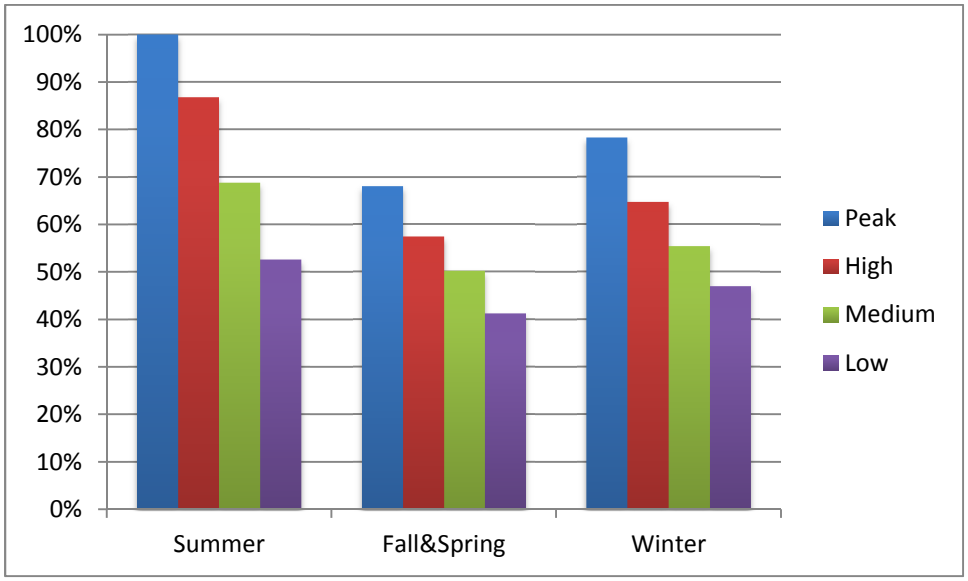

Fig. 5.2 Scaling of the load in each representative hour type

One of the important features of the SuperOPF is its ability to study the effects of environmental regulations on optimal generation investment. In that regard, the term “emissions price” is used in this paper to refer to an emissions tax or the permit-purchasing price in a cap-and-trade program.

For investment in new generators, five fuel types of generators are considered: coal, natural gas, solar, wind and nuclear. Total capacity addition limit for each type of generator is calculated based on the historical data and the estimation of the growth rate of each fuel type. The total capacity addition limit for each fuel type is listed in Table 5.1.

The SuperOPF takes into account generation marginal cost, maintenance costs, capital cost for building new plants and carrying charges. Capital recovery and fix cost for existing and new generators were obtained from [5] as shown in Table 5.2. It should be noted that the capital recovery for solar declines from $ 590,000 to $390,000 in 2032, since it is expected that the building cost for solar units will decrease in the future. To model DOE’s nuclear loan guaranty program, capital cost for nuclear generators is reduced [66]. Long run response to price (a.k.a., demand elasticity) is assumed to be -0.8 [67]. The growth of load is calculated based on the data obtained from *ERCOT Hourly Load Data Archives* [61].

TABLE 5.1
TOTAL TWO-DECADE CAPACITY-ADDITION LIMIT BY FUEL TYPE BY 2032

Fuel Type	Total capacity addition limit by 2032 (MW)
Coal	10,000
Natural Gas	33,000
Nuclear	5,000
Wind	16,000
Solar	9,700

TABLE 5.2
CAPITAL RECOVERY AND TOTAL FIX COSTS FOR DIFFERENT TYPE OF GENERATORS

Fuel Type	Capital Recovery ($/MW/Year)	Annual Total Fix Costs($/MW)
Coal	497,201	35,255
Natural Gas	181,824	20,661
Nuclear	470,226	95,571
Wind	392,322	20,661
Solar	520,000 (in 2012 and 2022) 390,000 (in 2032)	20,661

5.3 Description of the Cases

To assess the response of long-term generation investment to the future environment, an environment that is uncertain, studies are conducted using six possible 30-year futures and predictions of generation investment are made. Each future (case) consists of three simulation years: 2012, 2022 and 2032, an interval which is based on the assumption that each investment cycle takes ten years. For all the cases, the first cycle of generation investment starts in year 2012 and ends in 2022. The simulation year 2012 is assumed to have generation as built today.

The cases studied in this report are described as follows. The first case is referred to as the base case. In the base case, no environmental regulation or subsides for renewable energy is considered.

In the second case, a CO_2 emissions price is added to represent the cap-and-trade auctions for CO_2. This cap-and-trade auction for CO_2 is similar to that proposed by the Kerry-Lieberman Bill. This case is referred to as the cap-and-trade (C&T) case. In the C&T case, escalation of CO_2 prices is included, with the CO_2 price starting at 36.94 $/ton in 2022 and escalating to 60.18 $/ton in year 2032. Besides modeling CO_2 emissions prices, subsides for wind and solar generation are included. An incentive of 22 $/MW for wind and solar generation is added to model the Federal Renewable Electricity Production Tax Credit [69].

Similar to the C&T case, the third case also includes the same incentives for wind and solar generation. The incentives for wind and solar used in the third case are the same as those used in the K-L case. An EPA proposed rule aimed at regulating CO_2 emissions from power plants is included in the third case, a rule that is expected to be finalized later in 2012. This rule requires all new fossil-fuel-fired generation of 25 MW or more must emit no more than 1000 lbs of CO_2 per MWh. Since coal-fired plants cannot meet this standard, the standard effectively prohibits the construction of new coal plants. Therefore, in the third case, no new coal-fired plants can be built in 2022 and 2032. The third case is referred to as the EAP case.

All of the three cases are simulated with two different sets of gas prices, yielding six futures in total. The first set of gas prices is referred to as the high gas price set, which is 2.5 $/MMBTU in 2012, 7 $/MMBTU in 2022 and 14 $/MMBTU in 2032,. The gas price of 2.5 $/MMBTU modeled in 2012 is based on the assumption that the reserve of shale gas is large enough to keep the price

suppressed for 10 years. The shale gas is expected to be depleted in 2022 and therefore the gas price increases to7 $/MMBTU in the same year. Then in 2032, the gas price converges to the world price which is 14 $/MMBTU. The gas price of 14 $/MMBTU may seem large, but the gas price was in the neighborhood of 15 $/MMBTU in 2005.

The second set of gas price is referred to as low gas price set, which is 2.5 $/MMBTU in 2012, 4.77 $/MMBTU in 2022 and 5.86 $/MMBTU in 2032. This set of gas prices is estimated by the EIA [68].

Based on the different sets of gas prices used, the cases studied can be categorized into two groups. The cases that are run with the high gas price set are referred to as high-gas-price cases (HG) and similarly the cases that run with low-gas-price set (LG) are referred to as low gas price cases. The summary of modeling of each case and the two sets of natural gas prices are shown in Table 5.3 and Table 5.4.

TABLE 5.3
SUMMARY OF THE MODELING OF THE CASES

	Base Cases	C&T Cases	EPA Cases
CO2 emissions price	×	√	×
EPA Regulation	×	×	√
Incentives for wind and solar	×	√	√

TABLE 5.4
SUMMARY OF THE TWO SETS OF NATURAL GAS PRICES

	2012 ($/MMBTU)	2022 ($/MMBTU)	2032 ($/MMBTU)
High Gas Prices	2.50	7	14
Low Gas Prices	2.50	4.77	5.86

5.4 Results for Each Case

In this subsection, the effects that the six futures (cases) have on the investment and retirement of generation in the ERCOT system are studied and analyzed. The retirements and additions for the five fuel types—coal, natural gas, nuclear, wind and solar—considered in the investment study are shown in Fig. 5.3 to Fig. 5.7.

5.4.1 Natural Gas

Fig. 5.3 (a) and (b) show the retirements and additions for natural gas units. As shown in Fig. 5.3 (a), the C&T HG case has the largest capacity of natural gas retirement among all the cases, which is around 18.5 GW in 2022. This is the result of the high gas price (7 $/MMBTU) and CO_2 emissions penalties modeled in the C&T HG case, since together they increase the operational costs for natural gas units. Natural gas units are only built in the C&T LG case in 2032 which is about 17 GW, as shown in Fig. 5.3 (b). In 2022 in the C&T LG case, because of the wind and solar incentives, wind and solar are built to compensate for the retirement in natural gas and to serve the assumed growth in demand. Therefore no natural gas unit is built in 2022. In 2032, as the natural gas price continues to increase, building new natural gas units becomes more economical than dispatching existing natural gas units because, while new gas natural units are expensive to build, they are relatively inexpensive to operate. In 2032, wind and solar reach their building limits (which can be seen from Fig. 5.5 and Fig. 5.6), and the imposition of CO_2 emissions prices forces about 16 GW of coal to retire

by year 2032 (11.6 GW in 2022 and 4.4 GW in 2032), which is shown in Fig. 5.4. Therefore about 17 GW of natural gas is built in 2032 in the C&T LG case.

In the three HG cases, the high gas prices increase the operating costs and decrease the competitiveness of the natural gas units. Therefore no new natural gas unit is built in any of the HG case. For the base and EPA LG cases, where CO_2 emissions prices are not imposed, it is cheaper to dispatch existing coal units than building natural gas units. Therefore no natural gas unit is built in the base LG or the EPA LG case.

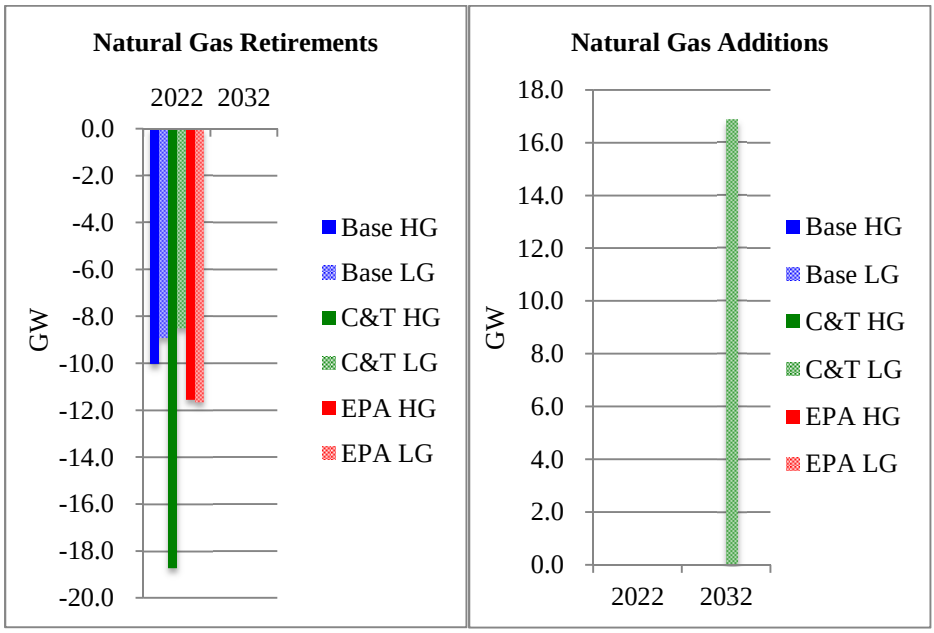

(a) Natural gas retirements (b) Natural gas additions

Fig. 5.3 Retirements and additions for natural gas units

5.4.2 Coal

The retirements for coal are shown in Fig. 5.4. It can be seen from Fig. 5.4 that the C&T LG case has the largest capacity of coal retirement, which is 11.5 GW in 2022 and 4.5 GW in 2032. Comparing the C&T LG case with the other

two LG cases, the imposition of CO_2 emissions penalties increases the operating cost for coal units; therefore more coal units are decommissioned in the C&T LG case. Similar reasoning maybe used to explain why more coal is decommissioned in the C&T LG case than that in the base HG and EPA HG case.

Comparing the C&T LG case with the C&T HG case, it can be seen that only about 0.5 GW of coal is retired in 2022 in the C&T HG case, which is less than 5% of the capacity of coal retired in 2022 in the C&T LG case. This is because the high natural gas price modeled in the C&T HG case increases the operating costs for natural gas units and results in the dispatching of more coal units. Therefore much less coal is decommissioned in the C&T HG case than that in the C&T LG case. No coal unit is built in any case, because coal units are expensive to build. To replace retired coal, wind and solar units are built in each case. Since more coal is retired in the C&T LG case, natural gas units are built in addition to the building of wind and solar units.

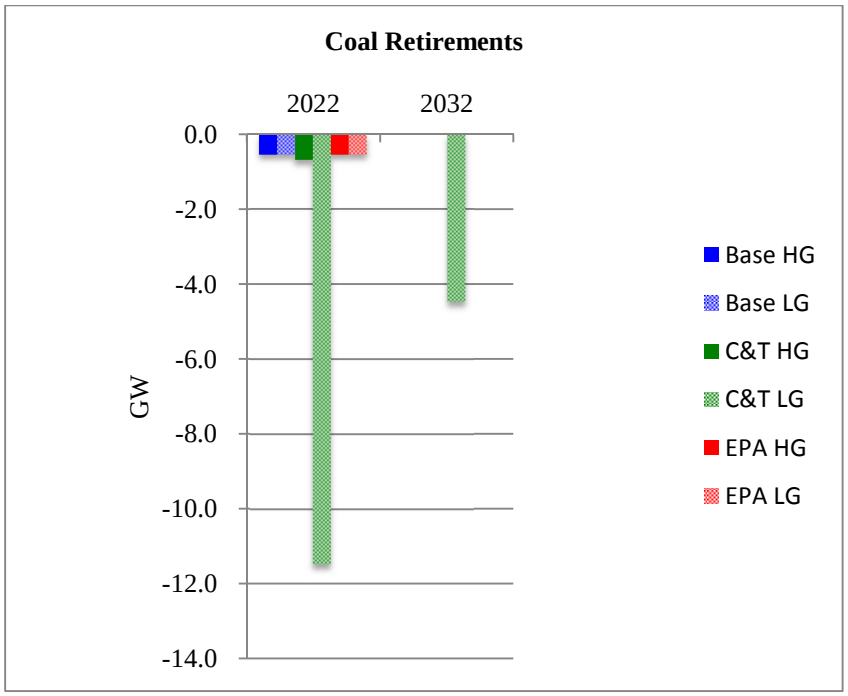

Fig. 5.4 Retirements and additions for coal units

5.4.3 Wind

The additions for wind generation are shown in Fig. 5.5. Since wind is cheap to operate, no wind unit is retired in any of the scenarios studied. In all the six scenarios, when the wind additions from both decades of the study are added, wind reaches its building limit by 2032. From Fig. 5.5, it can be noticed that the two C&T cases and the two EPA cases add the same wind capacity in 2022 and 2032, which is the result of the wind and solar incentives modeled in these four cases. In 2022, no wind unit is built in the base LG case while 1.3 GW is built in the base HG case. This is because more natural gas generation is dispatched in the base LG case since the natural gas price is lower in this case. Therefore no wind unit needs to be built in the base LG case in 2022.

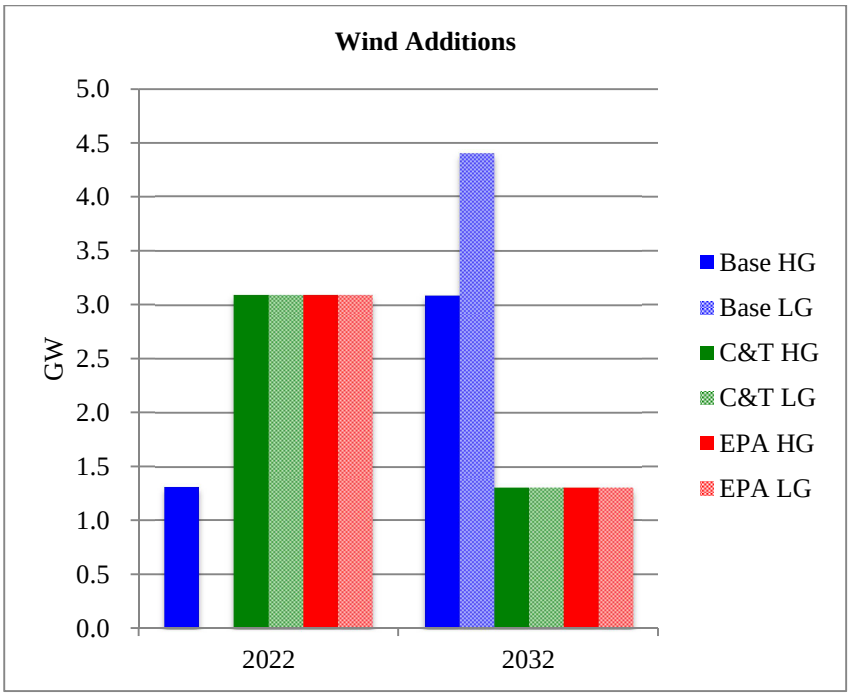

Fig. 5.5 Additions for wind units

5.4.4 Solar

The additions for solar generation in each year are depicted in Fig. 5.6. Except for the base LG case, solar reaches its maximum building limit in all of the other five cases. In the base LG case, natural gas prices are much lower than that in the base HG case in 2032; therefore more natural gas generation is dispatched and less solar is built in the LG base case than in the base HG case during the second decade of the study. Since no incentives are modeled in the base LG case, less solar is built in the base LG case than in either of the two-C&T or in either of the two-EPA cases. Meanwhile, for the two base cases and the two EPA cases, solar units are only built in the second decade of the study. This is the result of the projected reduction in the capital cost of solar and the corresponding decline in the capital recovery for solar in the second decade of study as shown in Table 5.2.

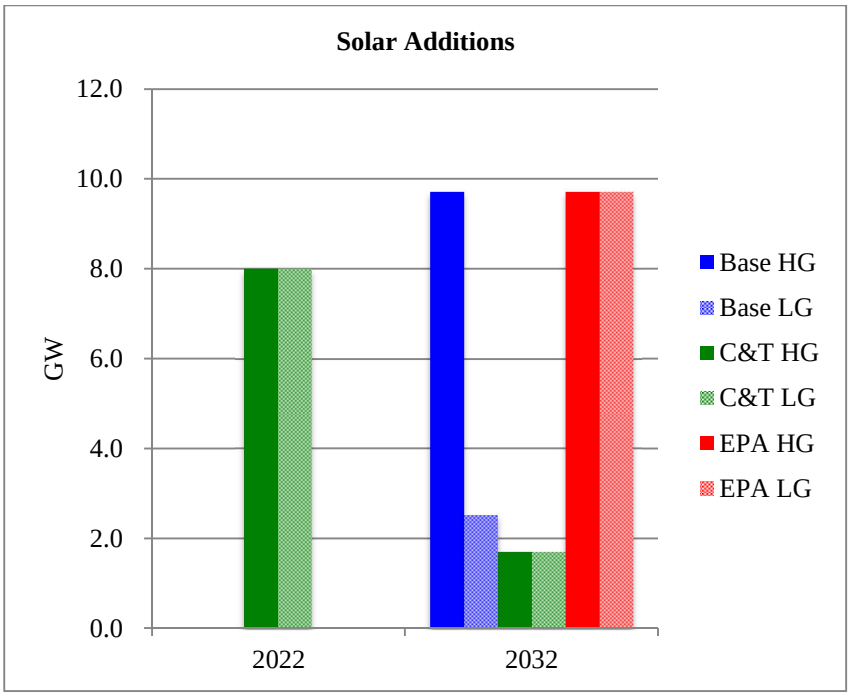

Fig. 5.6 Additions for solar units

5.4.5 Nuclear

The additions for nuclear are shown in Fig. 5.7. Since nuclear is cheap to operate, no nuclear unit is decommissioned in any case. As shown in Fig. 5.7, nuclear is only built in the HG cases, which is because more natural gas generation is dispatched in the LG cases and no nuclear unit needs to be built in the LG cases. Among the three HG cases, the C&T case has the largest addition of nuclear capacity. This is expected since the imposition of a CO_2 emissions prices and the positing of high gas price decreases the dispatch of coal and natural gas generation in the C&T HG case. As solar and wind reach their building limits in 2032, nuclear units need be built to serve the demand.

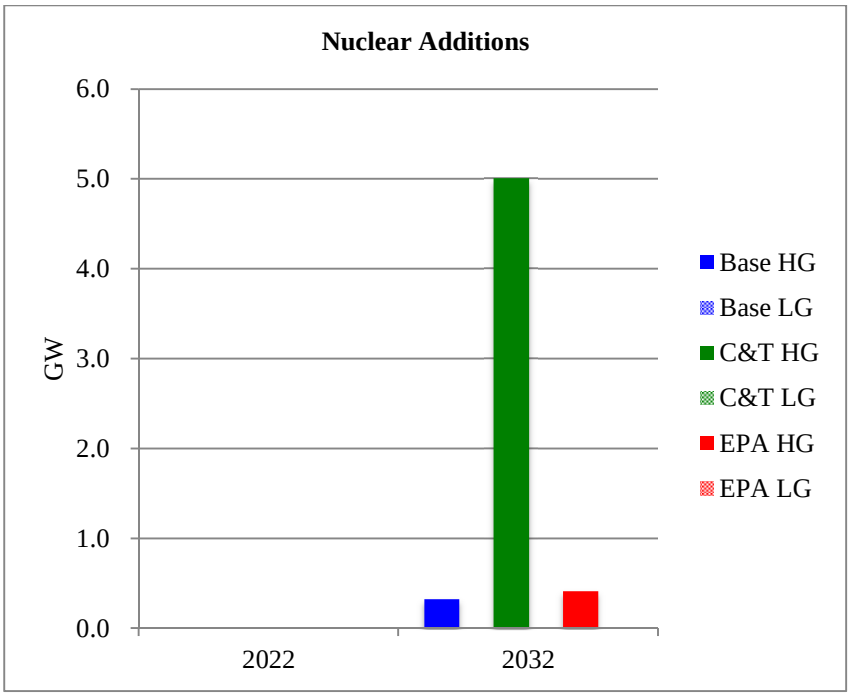

Fig. 5.7 Retirements and additions for nuclear units

5.4.6 Wholesale Prices, Total Energy Generated and Total CO_2 Emissions in the System

Fig. 5.8 to Fig. 5.9 show the total energy generated and average wholesale prices for each case. By 2032, as shown in Fig. 5.8, the three LG cases have higher total energy generated than the three HG cases. This result is consistent with the results for wholesale prices; as the wholesale prices in the HG cases are all higher than those in the LG cases by 2032, which can be seen in Fig. 5.9, long-term price response would cause demand to decrease in the HG cases. Among the three LG cases, the EPA case has the largest total energy generated by 2032, with the base case coming second and C&T case following next. This is also consistent with the results for wholesale prices. With CO_2 emission prices modeled, the C&T case has the highest wholesale prices among all the LG cases. The EPA LG case

has the lowest wholesale prices among the three LG cases, which is the result of the solar and wind incentives modeled in this case.

The similar pattern can be also found in the three HG cases: the C&T HG case has the lowest energy generated and highest wholesale prices. It is interesting to note that the wholesale prices and the energy generated in 2032 are very close in the base HG case and EPA HG case. In year 2032, in both of these two cases, wind and solar reach their building limits and the capacity of nuclear built is similar. Since no coal or natural gas units are built or retired in 2032 in these two cases, the generation mix in the two cases is very similar. This is why the wholesale prices and energy generated in these two cases are very close.

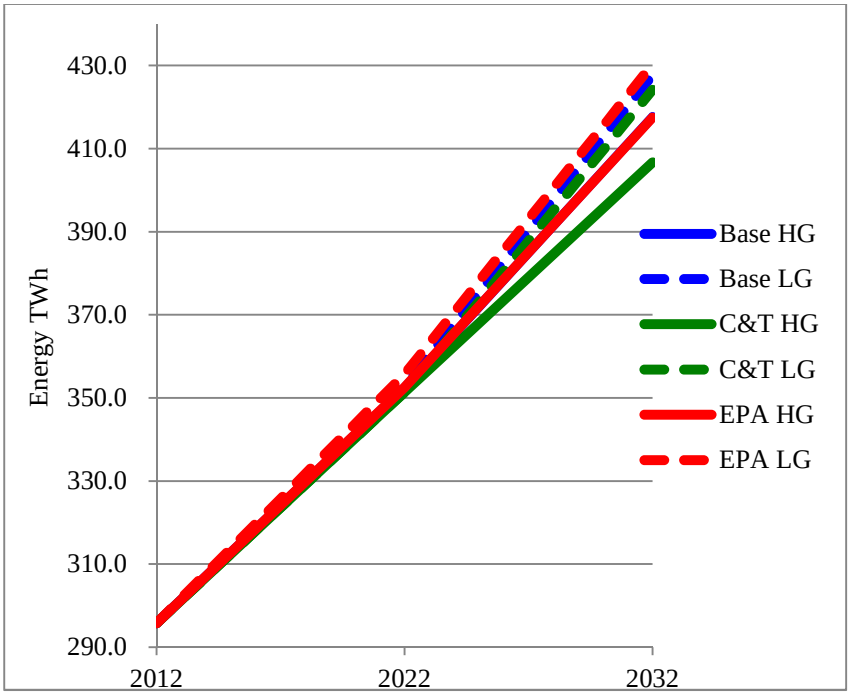

Fig. 5.8 Total energy generated in each case

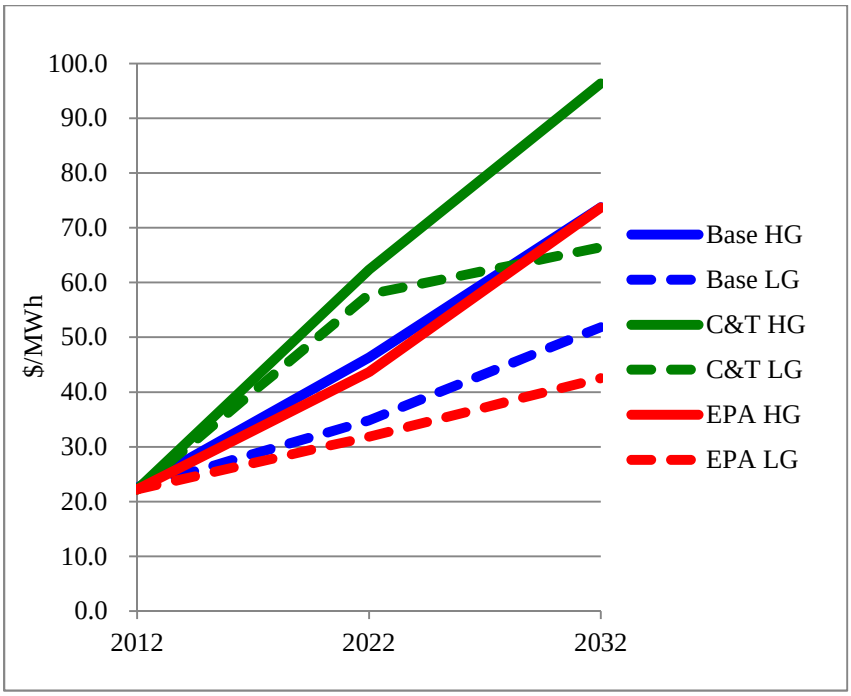

Fig. 5.9 Average wholesale prices for each case

The total CO_2 emissions in the system for each case are depicted in Fig. 5.10. Among all the six cases, the two C&T cases have the lowest total CO_2 emissions, which is the result of the CO_2 emissions penalties modeled in these two cases. The CO_2 emissions in the C&T HG case are higher than that in C&T LG case, which is because of the higher natural gas price modeled in the C&T HG case shifting power dispatch from future gas to existing coal. The total CO_2 emissions in the EPA LG case is lower than that in the LG base case. This is the result of the incentives for wind and solar modeled in the EPA LG case, The EPA regulation has no affects in the EPA LG case since the low natural gas price prevents coal from being built.

Comparing the HG base case with the EPA HG case, the total CO_2 emissions in the HG base case are higher in year 2022 but converge to the same level as that

in the EPA HG case in year 2032. In year 2022, more wind is built in the EPA HG case, which decreases the CO_2 emissions in the EPA HG case. However, in year 2032, wind and solar reach their building limit in both cases and similar capacity of nuclear is built in the two cases. Since no coal or natural gas unit is built or retired in 2032, the generation mix in the two base cases are very similar. Therefore, the total CO_2 emissions in the two base cases are close.

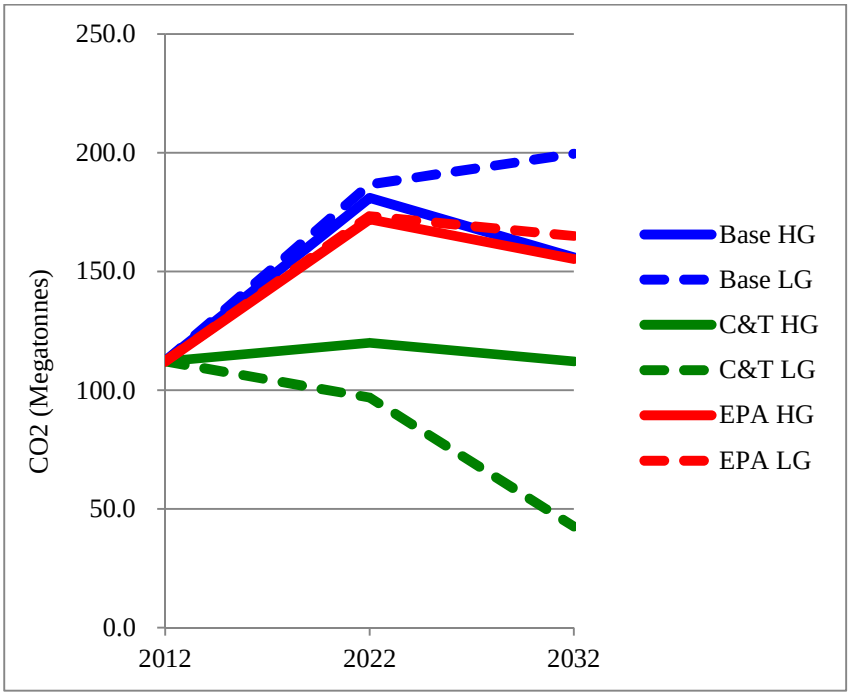

Fig. 5.10 Total CO_2 emissions in the system

CHAPTER 6 .

CONCLUSIONS AND FUTRUE WORKS

6.1 Conclusions

In this thesis, two possible solutions to improve the execution time of large-scale power system simulations are proposed and discussed. The first strategy is to implement a relatively new factorization method to speed up the solution of the sparse linear matrix equations. The other one is to use a small dc backbone equivalent of the large-scale power system but with reasonable accuracy. The major conclusions are drawn as follows:

- The performance of the multifrontal method is compared against the traditional LU factorization on different types of matrices characteristic of power-system simulations, as well as the matrices characteristic of some specialties outside the power system area. The comparison results demonstrate that the multifrontal method is superior to the traditional LU factorization on relative denser matrices but has poor performance on very sparse matrices that occur in power-system simulations. The result suggests that the implementation of multifrontal methods may not be an effective way to improve the execution time of large power system simulations and power system engineers should evaluate the performance of the multifrontal method before using it in their applications.
- A backbone equivalent for ERCOT system is generated using the modified Ward network reduction technique. In the equivalent, all generators in the original ERCOT system are retained integrally and the retained-line flows

in the reduced model exactly match those in the full model under the base case.

- Under changed generation cases, tests are conducted to quantify the differences (error) in retained-line flows between the reduced model and the full model. To study the relationship between the accuracy and size of the equivalent, equivalents with different sizes are generated and the errors in retained-line flow are studied. The results show that the discrepancy between the reduced model and full model decreases as more buses are retained in the equivalent.
- The accuracy of the equivalent is validated in the dc OPF based test. For the 424-bus equivalent, the dc OPF converges about 6 times faster than when using the full model. The errors in total cost, average LMP and generation dispatch by fuel type in the reduced model are calculated. The results demonstrate that the error in the equivalent is acceptable for OPF studies.
- The accuracy of the dc power flow model used for ERCOT equivalents is validated. Two different types of dc power flow models are studied, and the differences in the retained-line flows between the reduced dc model and the full ac model using the two models are quantified. The results show that the dc power flow model with zonal loss compensation is superior to classic dc power flow model for large-scale system.
- The 279-bus model is used in optimal generation investment planning study. Six possible 30-year-window futures and predictions are modeled to study the future generation investment and retirement under the impact of

different policies. The execution time for optimal generation investment planning is greatly reduced by using the 279-bus model.

- For fossil-fuel generation, new natural gas is only built in the C&T LG case, while the retirement of natural gas unit occurs in all the six scenarios. Coal units are not constructed in any of the scenarios. The retirement of coal is accelerated by possible CO_2 emissions regulations, production tax credits and the low natural gas prices.
- Investment in renewable sources is encouraged by high gas prices, CO_2 emissions regulations and the federal production tax credits. In all the scenarios, wind reaches its building limit by year 2032 (by adding the capacity additions in 2022 and 2032) and no existing wind unit is retired. For solar, except for the base LG case, solar reaches its maximum building limit in all of the other five cases. The building of nuclear units only occurs in the three HG cases, with the C&T HG case having the most capacity addition.
- Across all six scenarios, the three HG cases have higher electricity prices and lower total energy generation than the corresponding LG cases. The total system CO_2 emissions are lowest with the C&T LG case in which low gas price, cap-and-trade for CO_2 emissions and the production tax credits are modeled. The base LG case has the highest CO_2 emissions, since it is modeled with low natural gas prices and without environmental regulations.

6.2 Future Works

In this thesis, two possible strategies are introduced to improve the execution time for large system simulations. In addition to the work discussed in this thesis, the following work is suggested for future:

- For multifrontal methods, the results have shown that it is not efficient on very sparse matrices occurring in most of the power system simulations. However, for some rare cases, power system engineers may also encounter abnormally dense matrices, such as the 4578 node matrix used in the test which is an equivalent of a 60,000 node eastern interconnection system. In such circumstances, multifrontal methods may be a potential tool to speed up the large system simulations. Therefore, more testing can be done to compare the performance between multifrontal methods and the traditional LU factorization on matrices for a wider range of applications. The UMFPACK gain can be plotted versus the number of nonzeros per row in *L* and *U* factors to yield a more accurate prediction of the performance of multifrontal method. This plot can be used as a reference for engineers to check if the multifrontal methods can speed up their applications.
- The results show that UMFPACK gain is affected by the degree of sparsity (number of nonzeros per row) as well as sparsity pattern/topology (very approximately measured by the number of fill-ins). Futrue studies can be conducted to explore how the sparsity pattern affects the performance of a factorization algorithm.
- In the modified Ward equivalencing technique, the generators are moved based on electrical distance. More tests can be performed to study the

impact of the movement of generators on the accuracy of the equivalent. Furthermore, new criteria can be proposed to move the generators in the system integrally.

- In the optimal generation investment study, besides the fuel prices and environmental policies studied in this thesis, the impact of other factors on future generation mix, such as the impact of bulk energy storage and the intermittency in generation caused by high penetration of renewable energy, also requires studying. Therefore, more scenarios can be modeled to predict the impact of different factors on the future generation in the system.

REFERENCE

[1]. IPCC, “Intergovernmental panel for climate change fourth assessment report,” Cambridge Univ. Press, Cambridge, U.K., 2007.

[2]. N. Stern, The Economics of Climate Change: The Stern Review, Cambridge Univ. Press, Cambridge, U.K., 2007.

[3]. U.S Energy Information Administration, ”Emissions of greenhouse gases in the United States 2008,” Dec. 2009, Available: http://www.eia.doe.gov/oiaf/1605/ggrpt/pdf/0573(2008).pdf

[4]. Regional Greenhouse Gas Initiative, Inc., “Investment of proceeds from RGGI CO2 allowances,” Feb. 2011, Available: http://www.rggi.org/docs/Investment_of_RGGI_Allowance_Proceeds.pdf

[5]. William Schulze, et al., “Mapping energy futures using the SuperOPF Planning Tool: an integrated engineering, economic and environmental model,” Dec. 2011

[6]. J. Liu, “The multifrontal method for sparse matrix solution: theory and practice,” SIAM Rev., vol. 34, no. 1, pp. 82-109, 1992.

[7]. C. Ashcraft, R. Grimes, J. Lewis, B. Peyton, and H. Ssimon, “Progress in sparse matrix methods for large linear systems on vector supercomputers,” Internat. J. Supercomput. Appl., pp. 10-29, 1987.

[8]. B. Irons, “A frontal solution program for finite element analysis,” Internat. J. Numer. Methods Engrg., pp. 5-32, 1987.

[9]. R. Benner, G. Montry, and G. Weigand, “Concurrent multifrontal methods: shared memory, cache, and frontwidth issues,” Internat. J. Supercomput. Appl., pp. 26-44, 1987.

[10]. J. Reid, “TREESOLVE, a Fortran package for solving large sets of linear finite element equations,” Tech. Report CSS 155, Computer Sciences and Systems Division, AERE Harwell, Oxfordshire, UK, 1984.

[11]. A. Conn, N. Gould, M. Lescrenier, and PH. Toint, “Performance of a multifrontal scheme for partially separable optimization,” Tech. Report 88/4, Department of Combinatorics and Optimization, University of Waterloo, Waterloo, Ontario, Canada, 1989.

[12]. R. Lucas, “Solving planar systems of equations on distributed-memory multiprocessor,” Ph.D. thesis, De- partment of Electrical Engineering, Stanford University, Stanford, CA, 1987.

[13]. P. Amenstoy and R. Tilch, “Solving the compressible Navier-Stokes equations with finite elements using a multifrontal method,” Impact of Computing in Science and Engineering, pp. 93-107, 1989.

[14]. I. S. Duff and J. K. Reid, “The multifrontal solution of indefinite sparse symmetric linear equations,” ACM Trans. Math. Soft- ware, 9 (1983), pp. 302-325.

[15]. T. Davis and I. S. Duff, “A combined unifrontal/multifrontal method for unsymmetric sparse matrices,” ACM Trans. Math. Softw., vol. 25, no. 1, pp. 1-20, Mar. 2004.

[16]. W. M. CHAN and A. GEORGE, “A linear time implementation of the reverse Cuthill-Mckee algorithm,” BIT 20, 8–14, 1980.

[17]. T. Davis, “A column pre-ordering strategy for the unsymmetric-pattern multi-frontal method,” ACM Trans. Math. Softw., vol. 30, no. 2, pp. 165–195, Jun. 2004.

[18]. J.J. Dongarra, J. D. Croz, and S. Hammarling, “A set of level 3 basic linear algebra subprograms,” ACM Trans. Math. Softw. , vol 16, pp. 1-17, 1990.

[19]. C. Ashcraft, “The Influence of Relaxed Supernode Partitions on the Multifrontal Method,” ACM Trans. Math. Softw., vol. 15, no. 4, pp. 291–309, 1989.

[20]. T. Orfanogianni, and R. Bacher, “Using automatic code differentiation in power flow algorithms,” IEEE Trans. Power Syst., vol. 14, no. 1, pp.138–144, Feb. 1999.

[21]. J. Johnson, P. Vachranukunkiet, S. Tiwari, P. Nagvajara, and C.Nwankpa, “Performance analysis of load flow computation using FPGA,” Proc. 15th Power Systems Computation Conf., 2005.

[22]. S.K. Khaitan, J.D. McCalley, and Q. Chen, “Multifrontal Solver for Online Power System Time-Domain Simulation,” IEEE Trans. Power Syst., vol. 23, no. 4, pp. 1727-1737, 2008.

[23]. T. Davis, “Algorithm 832: UMFPACK—An unsymmetric-pattern multifrontal method,” ACM Trans. Math. Softw., vol. 30, no. 2, pp. 196–199, 2004.

[24]. C. A. Canizares, Z. T. Faur, and F. L. Alvarado, “Pflow: Continuation and direct methods to locate fold bifurcations in ac/dc/facts power systems-power flow,” Available: http://iliniza.uwaterloo.ca/"claudio/software/pflow. html.

[25]. T. A. Davis, CHOLMOD Version 1.0 User Guide, Dept. of Computer and Information Science and Engineering, Univ. Florida, Gainesville, 2005. [Online]. Available: http://www.cise.ufl.edu/research/sparse/cholmod.

[26]. LAPACK --- Linear Algebra PACKage. [Online]. Available: http://www.netlib.org/lapack/#_licensing

[27]. Gilbert, R. John, C. Moler, and R. Schreiber, “Sparse matrices in MATLAB: Design and implementation,” SIAM J. Matrix Anal. Appl., vol. 13, pp. 333–356, 1992.

[28]. A. J. Lamadrid, S. Maneevitjit, T. D. Mount, C. E. Murillo-Sanchez, R. J. Thomas, R. D. Zimmerman, “A `SuperOPF' Framework," CERTS Report, December 2008. [Online]. Available: http://certs.lbl.gov/pdf/superopf-framework.pdf.

[29]. T. A. DAVIS, “Users’ guide to the unsymmetric-pattern multifrontal package (UMFPACK, version 1.1),” Tech. Rep. TR-95-004, 1995

[30]. T. A. DAVIS, and I. S. DUFF, “An unsymmetric-pattern multifrontal method for sparse LU factorization,” SIAM J. Matrix Anal. Appl. 18, 1, 140–158,1997.

[31]. I. S. Duff, “Design features of a frontal code for solving sparse unsymmetric linear system out-of-core,” SIAM J. Sci.Comput. 5, 270-280.

[32]. T. A. Davis, and I. S. Duff, “An unsymmetric-pattern multifrontal method for sparse LU factorization,” SIAM Journal on Matrix Analysis and Applications, vol 18, no. 1, pp. 140-158, Jan. 1997.

[33]. T. Davis, P. Amestoy, and I. Duff, “Algorithm 837: AMD, an approximate minimum degree ordering algorithm,” ACM Trans. Math. Softw., vol. 30, no. 3, pp. 381–388, 2004.

[34]. J. Liu, “The role of elimination trees in sparse factorization,” SIAM J. Matrix Anal. Appl., 11 (1990), pp. 134-172.

[35]. C.C. Ashcraft, et al., “Progress in Sparse Matrix Method for Large Linear Systems On Vector Supercomputers,” International Journal of High Performance Computing Applications, 1987.

[36]. C. Ashcraft, “The Influence of Relaxed Supernode Partitions on the Multifrontal Method,” ACM Trans. Math. Softw., vol. 15, no. 4, pp. 291–309, 1989.

[37]. I. S. Duff and J. K. Reid, ”The multifrontal solution of indefinite sparse symmetic linear equations,” ACM Trans. Math. Softw., 9 (1983), pp. 302-325.

[38]. J. A. Geroge, and J. W H. Liu, Computer Solution of Large Sparse Positive Definite Systems, Prentice- Hall, Englewood Cliffs, NJ, 1981.

[39]. R. C. Whaley, A. Petitet, and J. Dongarra, "Automated empirical optimization of software and the ATLAS project," Parallel Computing, 27(1-2):3-35, 2001.

[40]. T. Davis and Y. Hu, “The University of Florida Sparse Matrix Collection, ” ACM Trans. Math. Softw., in press.

[41]. F. Ma and V. Vittal, “A hybrid dynamic equivalent using ANN-based boundary matching technique,” IEEE Trans. Power Syst., to be published.

[42]. P. Dimo, Nodal Analysis of Power Systems, Abacus Press, Kent, England, 1975.

[43]. W. F. Tinney and W. L. Powell, “The REI Approach to Power Network Equivalents,” IEEE PICA Conference Proceedings, Minneapolis, pp. 384-390, July 1983.

[44]. E. C. Housos, G. Irisarri, R. M. Porter and A. M. Sasson, “Steady State Network Equivalents for Power System Planning Applications,” IEEE Trans. Power App. Syst., vol. PAS-99, no. 6, Nov./Dec. 1980.

[45]. J. B. Ward, “Equivalent Circuits for Power Flow Studies,” AIEE Trans. Power Appl. Syst., vol. 68, pp. 373–382, 1949.

[46]. W. Snyder, “Load-Flow Equivalent Circuits–An Overview,” IEEE PES Winter Meeting, New York, Jan. 1972.

[47]. F.F. Wu and A. Monticelli, “Critical review of external network modelling for online security analysis,” Electrical power & energy systems, vol.5, no. 4, 1983.

[48]. S. Deckmann, A. Pizzolante, A. Monticelli, B. Stott, and O. Alsac, “Studies on Power System Load Flow Equivalencing,” IEEE Trans. Power App. Syst., vol. PAS-99, no. 6, pp. 2301–2310, Nov./Dec. 1980.

[49]. S. Deckmann, A. Pizzolante, A. Monticelli, B. Stott, and O. Alsac, “Numerical testing of power system load flow equivalencing,” IEEE Trans. Power App. Syst., vol. PAS-99, no. 6, pp. 2292–2300, Nov./Dec. 1980.

[50]. R. A. M. V. Amerongen and H. P. V. Meeteren, “A generalized Ward equivalent for security analysis,” SM, 455-5, p.1519, June. 1982

[51]. A. Monticelli, S. Deckmann, A. Garcia and B. Stott, “Real-time External Equivalents for Static Security Analysis,” IEEE Trans. Power App. Syst., vol. PAS-98, No. 2, pp. 498-508, Mar./Apr. 1979.

[52]. K. L. Lo, L. J. Peng, J. F. Macqueen, A. O. Ekwue and N. H. Dandachi,”Extended Ward equivalent of external system for on-line security analysis,”, IEE 2nd International Conference, Hong Kong, Dec. 1993

[53]. J. Machowski, A. Cichy, F. Gubina and P .Omahen, “External subsystem equivalent mode for steady-state and dynamic security assessment,” IEEE Trans. Power Sys., vol. 3, No. 4, Nov. 1988

[54]. L. A. Zhukov, “Construction of power system electromechanical equivalents,” Izv. Akad. Nauk SSSR, Energy. and Transp., No. 2, 1965.

[55]. E. H. Allen, J. H. Lang, and M. D. Ilic,"A Combined Equivalenced-Electric, Economic, and Market Representation of the Northeastern Power

Coordinating Council U.S. Electric Power Systems," IEEE Trans. Power Syst., vol. 23, no. 3, pp. 896-907, Aug. 2008.

[56]. H. K. Singh and S. C. Srivastava, “A Reduced Network Representation Suitable for Fast Nodal Price Calculations in Electricity Markets,” IEEE Power Engineering Society General Meeting, vol. 2, pp. 2070-2077, June 2005.

[57]. X. Cheng and T. J. Overbye, "PTDF-based Power System Equivalents," IEEE Trans. Power Syst., vol. 20, no. 4, pp. 1868-1876, Nov. 2005.

[58]. HyungSeon Oh, “A New Network Reduction Methodology for Power System Planning Studies,” IEEE Trans. Power Syst., vol. 25, no. 2, pp. 677-684, May 2010.

[59]. D. Shi and D. J. Tylavsky, "An Improved Bus Aggregation Technique for Generating Network Equivalents," IEEE PES General Meeting, July 2012, San Diego, USA.

[60]. D. Shi, et al., “Optimal generation investment planning: Pt. 1: Network Equivalents,” to be published.

[61]. ERCOT Hourly Load Data Archives, [Online]. Available: http://www.ercot.com/gridinfo/load/load_hist/.

[62]. R. Zimmerman, C. E. Murillo-Sanchez, and D. Gan, MATPOWER: A MATLAB Power System Simulation Package. Ithaca, NY, 2008. [Online]. Available: http://www.pserc.cornell.edu/matpower/.

[63]. The Mosek Optimization Tools Manual, [Online]. Available: http://docs.mosek.com/6.0/tools/index.html.

[64]. B. Scott, J. Jardim, and O. Alsac, “DC power flow revisited,” IEEE Trans. Power App. Syst., vol. 24, No. 3, pp. 1290-1300, Mar. 2009.

[65]. D. Shawhan, et al., “Engineering, economic, and environmental simulation of power-sector policies: a preliminary application to carbon dioxide, sulfur dioxide, and nitrogen oxide emission regulation,” Rensselaer Working Papers in Economics, 2012.

[66]. Loan Programs of Office, U.S. Department of Energy, [Online]. Available: https://lpo.energy.gov/?page_id=31

[67]. C. Dahl, A Survey of Energy Demand Elasticities in Support of the Development of the NEMS, 1993. [Online]. Available: ftp://eia.doe.gov/pub/oiaf/elasticitysurvey/elasticitysurvey_dahl.pdf.

[68]. EIA, ”Annual energy outlook 2012 with projections to 2035,” DOE/EIA-0383(2012), Jun. 2012. [Online]. Available: http://www.eia.gov/forecasts/aeo/pdf/0383(2012).pdf

[69]. Database of State Incentives for Renewables & Efficiency, [Online]. Available: http://dsireusa.org/incentives/incentive.cfm?Incentive_Code=US13F

[70]. W. F. Tinney and J. W. Walker, “Direct solutions of sparse network equations by optimally ordered triangular factorization,” Proc. of the IEEE, vol. 55, no. 11, pp. 1801-1809, November 1967.

[71]. A. Gupta, “Recent advances in direct methods for solving unsymmetric sparse systems of linear equations,” ACM Trans. Math. Softw., vol. 28, no. 3, pp. 301-324, September 2022.